CORA Cork Open Research Archive
Cartlann Taighde Oscailte Chorcaí

Title	Characterization of the impact of freezing on ripened Gouda cheese using small and large amplitude oscillatory shear rheology
Authors	Digvijay, Digvijay;Huppertz, Thom;Kelly, Alan L.;Lamichhane, Prabin
Publication date	2024-12-19
Original Citation	Digvijay, D., Huppertz, T., Kelly, A. L. and Lamichhane, P. (2024) 'Characterization of the impact of freezing on ripened Gouda cheese using small and large amplitude oscillatory shear rheology', Food Hydrocolloids, 162, 110980 (14pp). https://doi.org/10.1016/j.foodhyd.2024.110980
Type of publication	Article (peer-reviewed)
Link to publisher's version	10.1016/j.foodhyd.2024.110980
Rights	© 2024, Elsevier Ltd. All rights are reserved, including those for text and data mining, AI training, and similar technologies. This manuscript version is made available under the CC BY-NC-ND 4.0 license. - https://creativecommons.org/licenses/by-nc-nd/4.0/
Download date	2026-11-16 07:28:34
Item downloaded from	https://hdl.handle.net/10468/16831

UCC
University College Cork, Ireland
Coláiste na hOllscoile Corcaigh

Food Hydrocolloids

Characterisation of the impact of freezing on ripened Gouda cheese using small and large amplitude oscillatory shear rheology

--Manuscript Draft--

Manuscript Number:	FOODHYD-D-24-04005R1
Article Type:	Research paper
Keywords:	Cheese, Freezing, Rheology, Microstructure, LAOS, Frozen storage
Corresponding Author:	Prabin Lamichhane, Ph.D. Teagasc Food Research Centre Moorepark IRELAND
First Author:	Digvijay Digvijay
Order of Authors:	Digvijay Digvijay
	Thom Huppertz
	Alan L. Kelly
	Prabin Lamichhane, Ph.D.
Abstract:	In this study, small amplitude oscillatory shear rheology (SAOS) and large amplitude oscillatory shear rheology (LAOS) were applied as complementary techniques to map the impact of two different freezing schemes, i.e., multiple rapid freeze-thaw cycles (FTC; -18 ±1 to 6°C) and quiescent frozen storage (FrS; -18 ±1°C, 3-months), on rheological and microstructural properties of aged (9 months) Gouda cheese. The modes of impact of FTC and FrS treatments were different, and LAOS was found to be a powerful tool to quantify such differences at practical deformation scales. The activation energy (Ea) of flow calculated above and below the crossover temperature (53.2±1.6°C) and frequency-dependence of storage (G') modulus were used to quantify freezing-induced thermo-rheological changes in the SAOS region. At large incremental deformations (10-360%), freezing impacted the intracycle elastic (G'L, G'M) moduli and intracycle viscous (η'L, η'M) moduli, resulting in strain-dependent zones of strain-stiffening and shear-thinning in the cheese matrix. Micro-cracks observed by confocal laser scanning microscopy (CLSM) were consistent with observed changes in the linear and non-linear rheological responses. This study provides a critical understanding of differences in the effects of FTC and FrS-type treatments, pertinent to practical frozen storage scenarios of Gouda cheese and other semi-hard dairy matrices.
Suggested Reviewers:	Norbert Raak University of Copenhagen nr@food.ku.dk Expert on food structure and rheology
	Prateek Sharma, PhD Associate professor, Utah State University prateek.sharma@usu.edu Expert on Cheese structure-function relationships, Food structure design and its impact on functionality of dairy ingredients and products, Rheology of dairy products.
	Haotian Zheng, PhD Assistant Professor, NC State hzheng23@ncsu.edu Expert on Technical functionalities of food hydrocolloids Dairy ingredients manufacturing and application, food structure and texture design (for improved stability, physiological functionality, and mouthfeel) Rheology & Tribology Food digestion
	Sally Gras, PhD Professor, University of Melbourne sgras@unimelb.edu.au

Powered by Editorial Manager® and ProduXion Manager® from Aries Systems Corporation

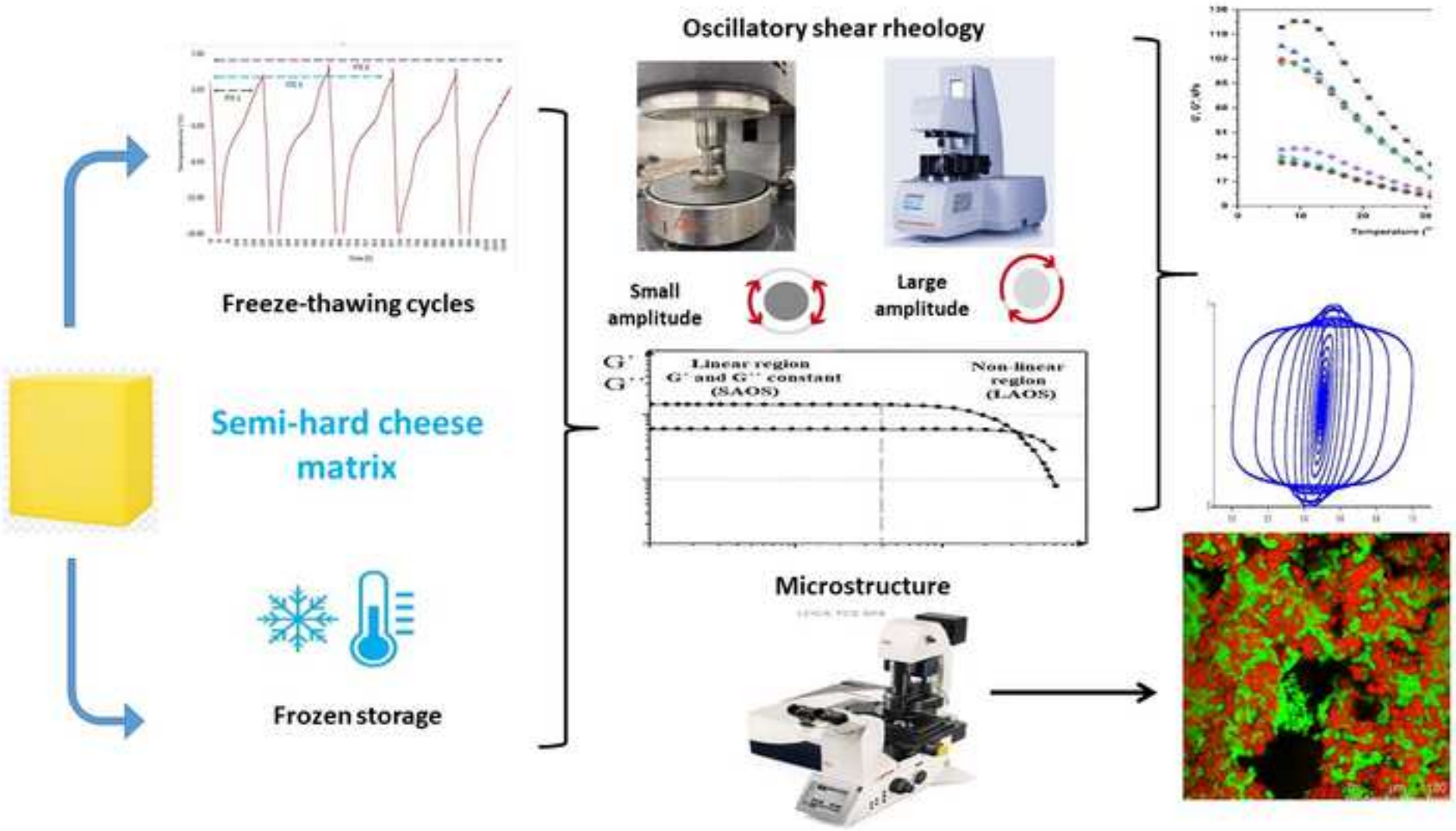
Wang, Q., Espert, M., Hernández, M., Salvador, A., & Sanz, T. (2024). Effect of cellulose ether emulsion and oleogel as healthy fat alternatives in cream cheese. Linear and nonlinear rheology, texture and sensory properties. *Food Hydrocolloids, 150*, 109740.

Highlights:

- Frozen storage and freeze-thaw cycles affect cheese rheology and microstructure
- Freezing treatments induced micro-cracks within the cheese matrix
- LAOS and SAOS could distinguish the impacts of freezing types on Gouda cheese
- Arrhenius and power-law models quantified the impact of freezing in the SAOS region
- LAOS quantifies the effect of freezing at practical deformation scales

Graphical Abstract

Click here to access/download;Graphical Abstract;Abstract-Gouda.jpg



Revised manuscript (Clean version) Click here to view linked References

Characterisation of the impact of freezing on ripened Gouda cheese using small and large amplitude oscillatory shear rheology

Digvijay [a, b], Thom Huppertz[b, c], Alan L. Kelly[b], Prabin Lamichhane[a*]

[a]Teagasc Food Research Center, Moorepark, Fermoy, Co. Cork, Ireland, P61 C996

[b]School of Food and Nutritional Sciences, University College Cork, Ireland, T12 YN60

[c] FrieslandCampina, Stationsplein 4, 3818, LE, Amersfoort, the Netherlands

***Author for correspondence: prabin.lamichhane@teagasc.ie**

Abstract

In this study, small amplitude oscillatory shear rheology (SAOS) and large amplitude oscillatory shear rheology (LAOS) were applied as complementary techniques to map the impact of two different freezing schemes, i.e., multiple rapid freeze-thaw cycles (FTC; -18 ±1 to 6°C) and quiescent frozen storage (FrS; -18 ±1°C, 3-months), on rheological and microstructural properties of aged (9 months) Gouda cheese. The modes of impact of FTC and FrS treatments were different, and LAOS was found to be a powerful tool to quantify such differences at practical deformation scales. The activation energy (Ea) of flow calculated above and below the crossover temperature (53.2±1.6°C) and frequency-dependence of storage (G') modulus were used to quantify freezing-induced thermo-rheological changes in the SAOS region. At large incremental deformations (10-360%), freezing impacted the intracycle elastic (G'_L, G'_M) moduli and intracycle viscous (η'_L, η'_M) moduli, resulting in strain-dependent zones of strain-stiffening and shear-thinning in the cheese matrix. Micro-cracks observed by confocal laser scanning microscopy (CLSM) were consistent with observed changes in the linear and non-linear rheological responses. This study provides a critical understanding of differences in the effects of FTC and FrS-type treatments, pertinent to practical frozen storage scenarios of Gouda cheese and other semi-hard dairy matrices.

1. Introduction

Global cheese production is on the rise, with an estimated growth of around 15% between 2020 to 2030, and is expected to reach a market value of $143 billion by 2032 (OECD/FAO, 2021; Shahbandeh, 2024). This growth is primarily driven by demand from food processors in China and other milk deficit countries in the Southeast Asia and the Middle East. To cater to the global markets, long distance frozen shipping of cheeses from primary producers in Europe and the USA is sometimes carried out to extend its techno-functional (cutting, slicing, shredding, grating, melting) shelf life (To, et al., 2020). Moreover, to address variability in cheese quality due to seasonal milk production systems (Timlin, et al., 2024), frozen storage is often preferred for bulk cheese procurement to provide greater flexibility in the duration of its usage. Also, to handle surplus production stock and stabilise demand-supply fluctuations, freezing may be applied to stop ripening at certain ages (Alinovi, Mucchetti, Wiking, & Corredig, 2021; Digvijay, Kelly, & Lamichhane, 2023).

During frozen storage of cheese, composition and microbial growth remain unchanged; however, texture-functional and overall sensory attributes can be adversely affected, and the extent of the effect varies based on the cheese type and composition (Digvijay, et al., 2023). Freezing causes localized concentration gradient formation, cryo-concentration of soluble components, dehydration of the casein-fat matrix, damage to the matrix due to ice recrystallization, and readjustments in the distribution of moisture and salts, as well as uneven reabsorption of moisture by the casein-fat network upon thawing (Alinovi, et al., 2021; Digvijay, et al., 2023; Meng-I Kuo & Gunasekaran, 2009; Reid & Yan, 2004; Verdini, Zorrilla, & Rubiolo, 2005). However, some prior studies have reported inconclusive results about the changes caused by freezing cheese (Fennema, 1972) and highlighted that the effect of freezing varies based on cheese type, size and rate of freezing used for the study (Oberg, Merrill, Brown,

& Richardson, 1992). Hence, cautious application of freezing is recommended for cheeses (Alinovi, et al., 2021; Bertola, Califano, Bevilacqua, & Zaritzky, 1996).

Both, low moisture part-skim (LMPS) and high moisture Mozzarella have been extensively investigated under different frozen storage conditions (Pax, et al., 2023; To, et al., 2020). However, the anisotropic nature of Mozzarella cheese restricts the generalization of obtained results to frozen storage of non-pasta filata type cheeses. Cheddar and Gouda-type cheeses are among the highest-selling semi-hard cheeses in the United States and Europe. The Netherlands is the largest exporter of Gouda-type Dutch cheeses, with a trade value of 1.26 billion euros in 2021 (Gelder, 2023). There is a growing interest in the prospects of freezing such cheeses at different ripening stages, targeting specific consumer markets and to stabilize supply-chain fluctuations (Alinovi, et al., 2021). Surprisingly, however, only one published report was found on the effects of frozen storage on Gouda cheese regarding its rheology and microstructure (Wiśniewska, Grześkiewicz, Jankowska, & Reps, 2012), and it provided limited information. Also, only a few studies have investigated the impact of freezing and frozen storage on other non-pasta filata type hard and semi-hard cheeses (Johnston, 2000; Kasprzak, Wendorff, & Chen, 1994; Reid, et al., 2004; Sommer, 1928). These studies, moreover, exclude the impacts of temperature fluctuations, which are unavoidable during frozen storage and shipping, on the cheese matrix.

Temperature fluctuations at sub-zero temperature conditions results in growth of ice-crystals by Ostwald-ripening, resulting in significant textural and rheological alterations in food and dairy products (Digvijay, et al., 2023). To date, however, critical understanding related to rheological and microstructural properties of semi-hard cheeses as affected by freezing, frozen-storage, and large-scale temperature fluctuations is limited. Hence, to address these research gaps, aged Gouda cheese (ripened for 9 months) was selected as a model semi-

hard matrix for the freezing study as it presented a unique consistency. The results can also help in understanding the effects of freezing on similar semi-hard dairy matrices.

In most of the published literature (Alinovi & Mucchetti, 2020; Alvarenga & Sousa, 2011; Meza, Verdini, & Rubiolo, 2011), SAOS analysis has been used to study the rheological characteristics of frozen-thawed cheeses, restricting the applied shear strain (γ) within the critical strain (γ_c) limit of the viscoelastic region (LVR). However, for many processing operations for cheese, like shredding, dicing, slicing, grating, and mastication, the deformation amplitude and its rate of application are multi-fold higher than the LVR and cross the γ_c of the SAOS region. As a result, linear viscoelastic characterization alone is insufficient to fully understand processing scenarios involving high deformation scales and rates, as SAOS analysis does not disrupt the 3D matrix of the cheese (Yildirim-Mavis, et al., 2022). Thus, for deformations beyond the LVR, nonlinear viscoelastic test protocols, i.e., large-amplitude oscillatory shear (LAOS), can provide useful insights on rheological phenomena (Ewoldt, Hosoi, & McKinley, 2008), such as shear-thinning or shear-thickening and strain-stiffening or strain-softening behaviour of Gouda type cheeses, and how these are affected by freezing treatments. Such rheological information can allow food manufacturers to optimise processing parameters while handling frozen-thawed cheeses.

Yildirim-Mavis, et al. (2022) used LAOS to study the rheological properties of Kashar cheese at high temperature and strain values and observed that the protein network resists progressive deformation of the cheese matrix, resulting in strain-stiffening and pseudoplastic behaviours. Recently, LAOS was used to study the structure development in Mozzarella cheese at different stages of its processing, highlighting the anisotropic dependence of strain stiffening behaviour of pasta filata type cheeses (Dahl, Gregersen, Andersen, Schulz, & Corredig, 2024). Piñeiro-Lago, et al. (2023) used LAOS to study the stress behaviour of acid-curd Spanish cheese (Afuega'l Pitu cheese, pH <4.6) and reported a pseudo-linearity in LAOS response of

cheese based on the dominance of rotation (stress-softening) over distortion observed in the normalised elliptical stress-strain plots. Correlation between the viscoelastic, sensory, and oral processing characteristics of Mozzarella, Cheddar, and processed cheeses have also been studied at large deformations, stressing upon the practicality of LAOS techniques (Melito, Daubert, & Foegeding, 2013). These reports indicate a positive trend in the utilization of this comprehensive rheological technique for understanding the viscoelasticity and structure-functionality of cheeses as affected by different processing conditions. However, unfortunately, no reports have detailed the impact of freezing Gouda cheeses at deformation scales relevant to real world usage conditions. Although, one reported study on the application of LAOS to Gouda-type cheese was found (Faber, Van Breemen, & McKinley, 2017). The study reported novel rheological explanations for firmness, rubberiness, and fluidization properties, as well as a new approach to measuring load-induced solid-liquid transitions in very young (3–14 days ripened) Gouda cheese with different fat levels. This, however, excludes mapping the large amount of viscoelastic transitions exhibited by aged Gouda cheese or the impact of freezing treatments.

Thus, the present study was designed to understand the impact of two different freezing schemes: (a) prolonged frozen storage (FrS) and (b) multiple freeze-thaw cycles (FTC) application on the thermo-rheological and microstructural properties of aged Gouda cheese using SAOS and LAOS techniques. The FTC application was done to simulate exaggerated temperature fluctuation conditions which could lead to the understanding of adverse effects on the semi-hard cheese matrix due to the loss of controlled frozen conditions or temperature fluctuations during commercial frozen storage and long-distance frozen shipping and retail distribution.

2. Materials and Methods

2.1 Cheese sampling and experimental design

Three different batches (vacuum-packed rectangular blocks ~ 15 kg/block/batch; total 45 kg) of industrial Gouda cheese samples manufactured on three different days of the same month were obtained from FrieslandCampina (Amersfoort, The Netherlands). Samples were ripened for a total of 9 months at 6°C in a temperature-controlled room. At the end of 9 months of ripening, each cheese block was portioned into 5 smaller blocks of ~ 3 kg, vacuum-packed, and stored at 6°C until subjected to freezing treatments, which completed within a week. Moisture, fat, salt, protein content and pH of ripened cheeses were determined as described by Page, et al. (2024). Samples were subjected to two different freezing schemes (FTC and FrS). From each batch of portioned cheeses, one randomly picked cheese block was used as an unfrozen control (6°C) sample and analysed within 48 hours of portioning; 3 cheese blocks were randomly picked for the multiple freeze-thaw cycles (FTC) study; and the remaining block of cheese was used for the prolonged frozen storage (FrS) study in a conventional chest freezer at -18±1°C for 3 months. All frozen samples were thawed at 6°C for 48 hours before the analysis and compared against the results of unfrozen control samples.

2.2 Application of multiple freeze-thaw cycles (FTC)

A forced convection air blast freezer (Roeder BGBF-15, Quipman Ireland Ltd.) was used to freeze the cheese samples at -18°C. A Testo 176T4 multichannel data logger (Titisee-Neustadt, Germany) with a chrome-aluminium K-type thermocouple (Fisher Scientific, UK) was used to monitor the temperature at the geometric center of a test Cheddar cheese sample of the same dimension and weight as Gouda cheese blocks, to estimate the freezing time needed to reach a core temperature of -18°C. It took 98±3 min for the 3-kg Cheddar block to reach -

18°C from 5°C (Fig. S1). Hence, the Gouda samples were stored in the blast freezer for 100 minutes to attain a core temperature of -18°C. After that, the samples were stored at 6°C for overnight thawing; this was counted as 1 FTC treatment. For FTC treatments, each block was given either 1 (FTC1), 3 (FTC3), or 5 (FTC5) continuous cycles of freezing-thawing treatments (Fig. S2). The application of freeze-thawing cycles were competed in 5 days. On day 1 of the week, FTC5 samples were subjected to FTC treatments in the blast freezer and, at day 3, FTC3 samples were added to the blast freezer, followed by FTC1 at day 5. Hence, all the FTC treatments were completed by day 5. Samples were analyzed after 48 hours of thawing at 6°C and all the tests were completed within the same week of thawing.

2.3 Small amplitude oscillatory shear (SAOS) rheology

SAOS analysis was performed using an ARG2 rheometer (TA Instruments, New Castle, USA) using a 20-mm serrated steel plate and base Peltier assembly. Cheese samples of 2.0 mm thickness and 20 mm diameter were obtained from the core of the blocks for temperature sweep and frequency sweep analysis. For the temperature sweep test, samples were subjected to 0.5% strain at a frequency 6.28 rad/s, which was within the cheese's LVR region obtained from strain sweep tests. The temperature ramp was performed at a rate of 2°C/min from 7 to 95°C. The outer sides of the samples were glazed with paraffin oil to avoid moisture loss during the tests. The activation energy of flow of the cheese matrix was calculated at two separate temperature ranges, 30-40°C and 70-80°C, to account for the contribution of the fat's liquid or solid state to structural strength. Arrhenius plot (eq. 1, 1a) at 30-40°C and 70-80°C were obtained using complex viscosity ($\eta^* = |G^*|/\omega$) and absolute temperature (T) to calculate the activation energy (E_a; kJ/mol) of cheese melting and deformation.

$$\eta^* = A \times e^{\left(\frac{-E_a}{R.T}\right)} \ldots\ldots\ldots (1)$$

193 $$\ln(\eta^*) = \ln(A) + (-\frac{E_a}{R}) \ln\left(\frac{1}{T}\right) \ldots\ldots (1a)$$

194 Where R (8.314 J $K^{-1}mol^{-1}$) is the universal gas constant, and A is Arrhenius constant.

195 The frequency sweep test was conducted at a constant strain value of 0.5% at 55°C, and the
196 results are interpreted at two different frequency ranges to account for strain application time
197 relevant to practical purposes, i.e., low frequency (LF); 0.06-9.958 rad/s (like spreading), and
198 high frequency (HF) application; 15-99 rad/s (cutting, grating, shredding). The frequency
199 dependence of mechanical moduli were analysed using a power-law model (eq. 2, 3) as
200 suggested by Tunick (2011).

201 $$G' = k_s (\omega)^S \ldots\ldots (2)$$

202 $$G'' = k_L (\omega)^L \ldots\ldots (3)$$

203 Where *S* and *L* are degree of frequency dependency for G' and G", respectively; and k_s and k_L
204 are consistency coefficients.

205

206 **2.4 Large amplitude oscillatory shear (LAOS) rheology**

207 LAOS analysis was performed using a strain-controlled Anton Paar Physica MCR 501
208 rheometer (Anton Paar GmbH, Austria) using the LAOS module in RheoCompass™ software
209 (v1.31). A parallel plate geometry using a sandblasted plate (PP50; diameter 50 mm) and a
210 base Peltier plate were used. Cheese samples of 50 mm diameter and 2 mm thickness, tempered
211 at 6°C for 24 hours (securely wrapped in aluminium foil to prevent moisture loss), were used
212 for the analysis. For every test condition used, i.e., frequency, temperature, strain, and sample
213 type, LAOS produces high-dimensional raw instrumental waveforms of stress-strain data.
214 Hence, for simplifying observations, the test was conducted only at a single frequency of 10
215 rad/s and temperature of 55°C, while using a range of strain values from 0.196 to 360% to

consider large-scale deformations. After sample loading, conditioning for 1 min at 55°C was performed, and the gap was maintained at 2 mm. For plotting Lissajous-Bowditch curves, data visualization, and similarity mapping of the rheological properties, VAOS open source software (source: GitHub at https://vis-au.github.io/vaos/) designed for studying viscoelasticity in soft materials was used (Madsen, Sode, Dahl, Corredig, & Schulz, 2022). A total of 300 points per quarter cycle were used for Fourier transformation and only the 3rd harmonic was considered for comparison of rheological responses (explained in section 2.4.1).

2.4.1 Mathematical background for LAOS analysis

For applied oscillatory strain (> γ_c) or stress > critical stress (σ_c), the output stress or strain waveforms are not sinusoidal due to large deformation amplitudes. However, the raw data can be used to extract useful rheological parameters with physical relevance to changes occurring in the cheese matrix. For the non-sinusoidal stress responses, the dynamic mechanical moduli can be expressed as a function of applied γ and ω, i.e., $G'(\gamma, \omega)$ and $G''(\gamma, \omega)$. The time series of raw instrumental strain and stress data is Fourier-transformed (FT) into frequency domain using infinite sum of sine and cosine functions at progressive harmonics (increasing ω), which constitutes the elastic (eq. 4) and viscous (eq. 5) signatures of the material (Ewoldt, Clasen, Hosoi, & McKinley, 2007).

$$\sigma = \gamma_0 \sum_{n\ odd} \left[G_n'(\omega, \gamma_o) \sin n\omega t + G_n^{"}(\omega, \gamma_o) \cos n\omega t \right] \ldots\ldots\ldots (4)$$

$$\sigma = \dot{\gamma}_0 \sum_{n\ odd} \left[\eta_n^{"}(\omega, \gamma_0) \sin n\omega t + \eta_n'(\omega, \gamma_0) \cos n\omega t \right] \ldots\ldots\ldots (5)$$

where G_n' and $G_n^{"}$ are Fourier coefficients (FC) representing elastic and viscous moduli of nth harmonic; $\eta_n^{"}$ and η_n' are FC representing dynamic viscosities of the nth harmonic; t is time (s); and n represents odd harmonics (1, 3, 5…) in the FT stress waveform and constitutes

useful rheological information. However, higher (>3) and even harmonics are assumed to represent more instrumental noise and testing artefacts e.g., wall slip, secondary flows (Läuger & Stettin, 2010), and thus have not been considered for viscoelastic measurements in this study. The generic nonlinear stress waveforms (eq. 4, 5) were subjected to orthogonal stress decomposition to obtain elastic (σ', Pa) and viscous ($\sigma", Pa$) components (eq. 6, 7)

$$\sigma' = \gamma_0 \sum_{n\ odd} G_n'(\omega, \gamma_0) \sin n\omega t \ \ldots\ldots\ldots (6)$$

$$\sigma" = \dot{\gamma_0} \sum_{n\ odd} G_n"(\omega, \gamma_0) \cos n\omega t \ \ldots\ldots\ldots (7)$$

These viscoelastic moduli are dependent on harmonics used in FT series and the number of harmonics generated are dependent on the applied strain and material properties. Cho, Hyun, Ahn, and Lee (2005) and Ewoldt, et al. (2008) addressed the strain-dependence of material viscoelasticity in the nonlinear region by using Chebyshev polynomials

$$\sigma' = \gamma_0 \sum_{n\ odd} e_n(\omega, \gamma_0) T_n\left(\frac{\gamma}{\gamma_0}\right) \ \ldots\ldots\ldots (8)$$

$$\sigma" = \dot{\gamma_0} \sum_{n\ odd} v_n(\omega, \gamma_0) T_n\left(\frac{\dot{\gamma}}{\dot{\gamma_0}}\right) \ldots\ldots\ldots (9)$$

where, for the n^{th} order harmonic, $e_n(\omega, \gamma_0)$ and $v_n(\omega, \gamma_0)$ are elastic and viscous Chebyshev coefficients, respectively at a given ω and γ_0; and T_n is Chebyshev polynomial of n^{th} order. The relationship between Chebyshev and Fourier coefficients (G_n' and $G_n"$) was established (eq. 10) by Ewoldt, et al. (2008) as:

$$e_n = G_n'(-1)^{\frac{(n-1)}{2}} \text{ and } v_n = \eta_n' = \frac{G_n"}{\omega} \ \ldots\ldots\ldots (10)$$

In this study, only the 3rd order elastic and viscous Chebyshev coefficients were considered for viscoelastic fingerprinting during the SAOS to LAOS transition. Non-linear rheological signatures like intracycle minimum strain (G_M') and large strain (G_L') moduli were obtained from the elastic Chebyshev coefficient e_n by calculating first degree derivative at $\gamma =$

0 and $\gamma = \gamma_0$ based on a deconvoluted stress-strain equation; similarly, intracycle instantaneous viscosity at minimum strain-rate ($\eta'_M;\ \dot{\gamma} = 0$) and large strain-rate ($\eta'_L;\ \dot{\gamma} = \dot{\gamma}_0$) were calculated based on the first degree derivative of the stress-strain rate equation. The parameters G'_L and G'_M refer to intracycle values of elastic modulus at the highest and lowest values of intracycle oscillatory strain application on a sample; this indicates the non-linearity expressed by a samples in terms of ratio (eq. 11) like strain-stiffening (S>0) or strain-softening (S<0). Similarly, η'_L and η'_M correspond to changes in the viscosity of a sample during intracycle strain application and explains shear-thickening (T>0) or shear-thinning (T <0) behaviour (eq. 12) of a sample (Ewoldt, et al., 2008; Seighalani & Joyner, 2019):

$$S(\omega, \gamma_0) = (G'_L - G'_M)/G'_L \ldots\ldots\ldots \quad (11)$$

$$T(\omega, \dot{\gamma}_0) = (\eta'_L - \eta'_M)/\eta'_L \ldots\ldots\ldots \quad (12)$$

Visualization of nonlinear responses was done by plotting normalized intracycle stress (σ) vs. strain (γ), and stress (σ) vs. strain rate ($\dot{\gamma}$) data as elastic and viscous Lissajous-Bowditch (LB) curves, respectively. On an elastic LB plot, at a fixed frequency and temperature, a perfect straight line indicates purely elastic material response whereas a perfect circle indicates purely viscous response. On a viscous LB plot, a purely viscous material is a perfect straight line where as purely elastic response is indicated by a perfect circle. However, a viscoelastic material response is indicated by elliptical shapes with short or long minor axis depending upon whether the material is viscoelastic solid or liquid on an elastic LB plot, respectively (Ewoldt, 2013).

2.5 Visualization of cheese microstructure using confocal laser scanning microscopy (CLSM)

The microstructure of cheese was visualised using a Leica TCS SP5 confocal laser scanning microscope (Leica Microsystems CMS GmbH) as described by Lamichhane, Sharma, Kennedy, Kelly, and Sheehan (2019), with slight modifications. Imaging was conducted with a 20×/0.70 oil immersion objective and a pinhole diameter set to 60.47 au. A digital zoom of 2× was used for all the imaging. Fast Green FCF was excited at 633 nm with a He/Ne laser, and its emission filter was set at 650 to 705 nm. Nile Red was excited at 488 nm with a diode-pumped solid-state laser, and its emission filter was set at 563 to 610 nm. Digital images, 1,024 × 1,024 pixels in size, were acquired using Leica LAS AV software (Leica Microsystems CMS GmbH), with each line averaged four times to improve the signal-to-noise ratio. Each sample was prepared in triplicate, and at least four different areas of each replica were imaged to ensure that images were representative. ImageJ image analysis software package (ImageJ, National Institutes of Health, USA) was used for processing of the micrograph in 8-bit image and for segmentation using color thresholding.

2.6 Statistical analysis

SPSS (Version 27) was used to determine significant differences between the results of rheological analysis at 5% level of significance using one-way analysis of variance (ANOVA) and Tukey's multiple comparison tests was used for paired comparison of treatment means at a 5% level of significance. Two-way ANOVA was used to compare the frequency-dependency of mechanical moduli at high and low frequencies among different FTC and FrS treatments, along with their interactive effects. For each trial, all the analysis were performed at least in triplicate.

3 Results and discussion

3.1 Cheese composition

Gouda cheese samples at the end of ripening and before any freezing treatments (control samples) had on average 41.4±0.6% moisture, 22.5±0.3% protein, 29.2±0.2% fat, 1.6±0.08% salt, and a pH of 5.45±0.02. Freeze-thawing cycles (FTC) and frozen storage (FrS) did not significantly affect cheese composition (Table S1). Similar observations have also been reported for frozen storage studies conducted on other cheese types (Alvarenga, et al., 2011; Van Hekken, Tunick, & Park, 2005).

3.2 Impact of freezing on cheese microstructure

CLSM micrographs (Fig. 1) were subjected to 8-bit image transformation and color thresholding to highlight the microscale gaps created during FTC and FrS treatments. The control sample had a typical cheese microstructure with an interspersed and embedded fat phase in a protein matrix with overall smooth microstructure. The color thresholding indicated minimum empty space (indicated as white patches) as compared to FTC and FrS, which could be micro air pockets left even after cheese pressing during manufacturing. As FTC progressed, changes in micro-gaps can be observed as increased area of white patches. The 8-bit images also indicated more roughening of microstructure with incremental FTC; this could be due to discontinuities created by movement of the water phase during repeated freeze-thawing.

From a microstructural perspective, even a single freeze-thaw cycle had an observable impact. For FTC3, FTC5 and FrS samples, the micro-gaps were comparable, although micro cracks more broader and less in number were prevalent in FTC5 and FrS treatments. This suggests that more water phase pooling and ice recrystallization occurs during repeated freeze-thawing treatments. The FrS treatment created a coarser microstructure with broad empty channels, and similar to this observation, Alinovi, Corredig, Mucchetti, and Carini (2020)

reported the formation of large serum channels in frozen stored (-18°C, 1-4 months) high-moisture Mozzarella, where dehydration of casein and structural expansion due to ice crystal formation were the underlined cause. Also, the minute variation in the microstructure of FrS could be related to the longer exposure of the casein network to cryo-concentrated solute phase leading to changes as discussed in Section 3.5.1. These differences in microstructure relates well to the differences in the diminished thermo-rheological responses obtained through SAOS and LAOS analysis.

Freezing-induced microstructural cracks of varying magnitudes have been reported for Cheddar (Reid, et al., 2004), LMPS Mozzarella (Meng-I Kuo, et al., 2009; Pax, et al., 2023) and ewe's milk cheese (Fontecha, Kaláb, Medina, Peláez, & Juárez, 1996) but no reported study on the microstructure of frozen Gouda cheese or other Dutch cheeses could be found. A longer duration of frozen storage (-20°C, 60 days) was reported to cause a honeycomb-like microstructure with microscale cracks in Mozzarella cheese, which were not observed in very short term frozen-stored (-15°C, 180 min) Mozzarella (Ribero, Rubiolo, & Zorrilla, 2009). However, the pasta-filata process used in the manufacturing of Mozzarella cheese restricts the microstructural comparison with Gouda cheese matrix used in the current study. The scale of differences in micro cracks observed in the reported studies could be due to the differences in cheese type and imaging techniques used like scanning electron microscopy (SEM), cryo-SEM, and transmission electron microscopy (TEM), which may induce artefacts due to sample preparation steps, unlike CLSM.

3.3 Viscoelastic properties measured using SAOS rheology

3.3.1 Impact of freezing on the mechanical moduli (G' and G") of cheese during temperature and frequency sweep tests

Viscoelastic responses of the aged Gouda cheese samples within the LVR range were evaluated by temperature and frequency sweep tests. Unfrozen control Gouda samples had higher average G' and G" values (kPa) throughout the temperature range of 7-90°C with notable differences observed at lower temperatures (< 50°C) as compared to FTC and FrS samples (Fig. 2a, 2b). Softening of the cheese matrix upon heating is an obvious thermo-physical change, primarily due to melting of fat, disruption of intra- and inter-protein cross linkages, and heat-induced mobility of moisture and fat in the matrix (Lamichhane, Kelly, & Sheehan, 2018). However, the lower average G' and G" moduli in FTC and FrS samples indicate freezing-induced changes in the structural strength of the cheese matrix. Also, it was observed that FTC treatments, which mimic large-scale temperature shock expected during temperature abuse in long distance shipping and retail distribution, impacted the cheese matrix differently than prolonged and quiescent frozen storage. The FrS treatment caused more loss of elastic characteristics of Gouda cheese than the FTC treatments, which countered the assumption that FTC would result in large-scale macroscopic structural changes in the cheese matrix.

The G' and G" values were statistically analysed at 10, 30, and 50°C (Table 1) and both moduli were significantly lower ($P<0.05$) for FrS samples compared to FTC and control samples. For G' values, no statistical difference was found within FTC samples except at 30°C. For G" values, minor differences within FTC samples were observed at 50°C, but these did not significantly differ from the FrS treatment. Overall, a decreasing trend for G' and G" moduli were observed for any freezing treatment applied. A progressive number of freeze thaw cycles did not change the rheological attributes and the rheological impact created in the first FTC remained mostly constant during further FTC application. One possible explanation for this could be the higher rate of cooling achieved using a blast freezer during the rapid FTC treatments i.e., 0.24°C/min as compared to the much slower cooling rate (0.035°C/min) to

384 which FrS samples were subjected while freezing to -18°C prior to frozen storage (Fig. S1).
385 Fontecha, et al. (1996) reported similar findings upon freezing a semi-hard cheese matrix from
386 ovine milk where slow freezing and prolonged frozen storage (-18°C; 4 months) resulted in a
387 pronounced decline in the shear strength and firmness of the cheese structure. Reid, et al. (2004)
388 studied freezing of Cheddar cheese (36-39% moisture) using different fast freezing methods
389 and reported a significant decline in shear strength of all the frozen samples, irrespective of
390 freezing rates used. However, the greater decline in mechanical moduli for FrS samples as
391 compared to FTC could be attributed to the fact that longer duration of frozen storage might
392 provide sufficient time for achieving a moisture-mineral redistribution equilibrium between the
393 regions of concentrated unfrozen serum phase and the casein matrix. Fennema (1972) also
394 highlighted the fact that a longer duration of frozen storage, instead of the freezing process
395 alone, can induce destabilization of proteins.

396 Also, freezing and frozen storage induced changes occurring in the hydration status of the
397 intact and proteolysed fractions of the caseins might also impact the mechanical response of
398 the cheese matrix (McMahon & Oberg, 2017). The hydration behaviour of intact casein
399 micelles indicated that unit mass of casein can associate with ~3.3 g of water, of which ~15%
400 is non-freezable water (primary hydration water or bound water), ~25-30% of water is
401 associated with κ-casein and ~55-60% is physically entrapped by the porous casein micelle
402 (Huppertz, et al., 2017). In aged Gouda cheese, however, extended ripening could lead to a
403 mixture of intact and proteolysed caseins as ~70-80% of α_{s1}-casein and ~50-60% of β-casein
404 is hydrolysed at the end of 6 month of ripening (Berg & Koning, 1990); thus, presenting a blend
405 of water holding capacities of proteins and peptides, with a possible shift in the entrapped
406 fraction of moisture. Buaynov and Buaynova (2016) reported the hydration status of proteins
407 in semi-hard variety of cheeses (~ 44% moisture, ~25% protein) and, based on gross
408 composition, it was observed that ~1.8 g of water was available per gram of cheese protein, of

409 which ~ 0.48-0.54 g g^{-1} protein was termed as bound water or the water fraction constituting
410 mono- and multi-layer hydration associated with the proteolysed caseins, when measured at 0
411 to -10ºC. This is in agreement with the hydration results for intact casein micelles by Huppertz,
412 et al. (2017). However, at -20ºC, the bound water fraction slightly reduced to ~0.39 g g^{-1} of
413 protein, which was attributed to a further crystallization of some multilayer water (binding
414 energy <21.80 kJ/kg moisture) attached at a relatively distant layer from the mono-layer water
415 in cheese proteins (Buaynov, et al., 2016). However, this counters the established notion of
416 bound water as unfreezable water (Tomaszewska-Gras, et al., 2019), but such differences in
417 the hydration behaviour of intact and proteolyticaly broken down caseins could be due to
418 inherent differences in their structural organisation.

419 Upon freezing cheeses, the solubilized minerals (Ca and P), non-protein and amino acids
420 nitrogen, organic acids, and ions (Na^+ and Cl^-) are freeze-concentrated in the serum phase,
421 leading to reduced pH, increased ionic strength and osmotic pressure around the hydrolysed
422 caseins (Reid, et al., 2004). Such changes could result in the dehydration of proteins (Alinovi
423 & Mucchetti, 2020). It has been indicated that partial removal of entrapped moisture from the
424 casein micelle structure can occur upon increased osmotic stress or ultracentrifugation for
425 longer periods (Huppertz, et al., 2017). Such moisture redistribution could happen more during
426 the FrS (longer moisture equilibration time i.e., 90 days at -18°C) treatment than rapid FTC
427 treatments; thus, a more dehydrated protein network could lead to lower G' and G" values in
428 FrS samples as compared to FTC and control samples. M-I Kuo and Gunasekaran (2003) and
429 Guinee and Fox (2017) also reported the possibility of a partially dehydrated and weaker casein
430 matrix in freeze-thawed cheeses. Similar findings on the behaviour of casein micelles under
431 high osmotic stresses have also been reported by Famelart, Le Graet, and Raulot (1999).

432 The rapid FTC treatments seems to freeze-thaw and refreeze only the serum moisture
433 (freezable moisture) and apparently little to no movement of multi-layered water occurs in this

short duration, hence, the hydration status of proteolysed caseins is not changed to the same extent as in the case of FrS treatment. The decline in the G' and G" values in the FTC samples could exclusively be a result of physical expansion of the matrix due to water and fat crystallization, as observed from the CLSM micrographs (Fig. 1) . Van Hekken, et al. (2005) reported a reduction in viscoelastic properties upon very short term frozen storage (2 days, -20 ºC) of soft caprine milk cheeses, hence, the impact of FTC treatments seems to remain more or less similar to other cheese matrixes as well; but, there is a gap in such published reports.

3.3.2 Activation energy (E_a) of flow and frequency dependence of mechanical moduli in the SAOS region

Microstructural changes and flow of the cheese matrix upon heating are an important functional and rheological attribute. The changes in δ (in rad; ratio of G"/G') during temperature sweep analysis indicates relaxation of intra- and inter protein-protein, protein-peptide and peptide-peptide bonds, and the maximum value of δ (δ_{max} at temperature $T_{\delta\text{-}max}$; °C) is also used to infer the melt or flow behaviour of cheeses (Sharma, Munro, Dessev, & Wiles, 2016). In the present study, however, no significant differences in δ_{max} and $T_{\delta\text{-}max}$ values were observed (Table 2) for any freezing treatments. As an alternative approach, Joyner (2019) reported that the thermo-rheological flow of materials can be comprehensively explained using structural rigidity (G*; complex modulus) or deformability (η^*; complex viscosity) indices. Thus, the activation energy (E_a, kJ/mol) of the cheese matrix, i.e., the energy required for its deformation and flow, was calculated, as it can account for the indices like G* or η^* (see eq. 1, 1a).

The contribution of fat to network strength is highly temperature dependent and the mechanical response of the cheese matrix rapidly declined (Fig. 2c) after the onset, until the

458 completion of fat melting in the range 30-40°C, and also due to limited softening of protein
459 network. Freezing impacts the polymorphic and crystallization status of fats and modifies the
460 physical protein-fat interaction behaviour (Alinovi & Mucchetti, 2020; Buldo, Andersen, &
461 Wiking, 2013). A typical range for latent heat of fusion of bovine milk fat ranges between 70-
462 80 J/g of fat (Tunick, 2010). Thus, to account for such factors, E_a before (E_a-t; 30-40°C) and
463 after (E_a-T; 70-80°C) the complete liquefaction of fat was calculated. The E_a-t values for
464 control, FTC and FrS cheese samples were in the range 100-110 kJ/mol and did not
465 significantly differ (Table 2, Fig. S3). Similar E_a values (100-150 kJ/mol at 30-45°C) were
466 reported for Cheddar and Mozzarella type cheeses by Tunick (2010). At higher temperatures
467 (70-80°C), the overall average E_a-T significantly ($p < 0.05$) decreased to ~27-48 kJ/mol for all
468 the samples, which is expected due to the complete loss of structure-forming ability of the fat
469 component (Lamichhane, et al., 2018). However, in this temperature range, the E_a for FTC or
470 FrS samples were higher than for the control samples. This effect could be due to the partial
471 dehydration of the protein network (discussed in previous section), which might present higher
472 resistance to initiate an actual flow due to the loss of lubrication (from fat, moisture), and
473 polymorphic transitions like sintering of fat crystals could have altered the environment around
474 the protein phase (Buldo, et al., 2013).

475 Udyarajan, Horne, and Lucey (2007) reported the possibility of heat-induced associations
476 at high temperatures (80-90°C) within a residual protein network by binding of some calcium
477 and phosphate ions as insoluble calcium precipitates, as observed from the increased elastic
478 properties of Cheddar cheese at 80-90°C. Also, it appears that, in the low temperature (30-
479 40°C) region, a pronounced effect of fat melting on mechanical moduli could mask the actual
480 impact of freezing treatments on the protein bonds. This is evident from no significant change
481 (Table 2) in the crossover temperature (53.2±1.6°C) for any freezing treatments, which strongly

indicates that the fat phase could actually provide a cushioning effect during network compression and expansion. Similar observations on thermo-rheological response during melting of fat free cheeses were reported by Lucey, Johnson, and Horne (2003), where relaxation of protein bonds in cheese started at temperatures >40°C. Thus, it appears that measuring E_a of freeze-thawed cheeses at temperatures above the complete liquefaction of fat could be more useful in measuring the impact of freezing on the protein matrix. Tunick (2010) reported E_a (at 30-45°C) values of 30-60 kJ/mol for non-melting caprine cheese and Queso Fresco cheeses, and E_a >180 kJ/mol for rapidly flowable Parmesan (very hard) cheese. This indicates that the high E_a only depicts an initial higher resistance in initiating the flow and deformation; however, it does not indicate the extent of melting a cheese matrix can achieve when supplied with energy >>E_a.

A frequency sweep analysis was done at 55°C (closer to the crossover temperature) in order to avoid structural contribution from the solid fat, ensuring sufficiently softened protein phase and yet avoiding major heat-induced changes in the cheese matrix. This temperature is also close to the practical consumption temperatures of cheeses. Power-law fitting was performed at low frequency (LF: 0.06-9.958 rad/s) and at high frequency (HF: 15-99 rad/s) to understand the frequency dependency of G' and G" (Fig. 2d, Table S2). The G' value was found to be more sensitive to frequency changes than G" for all the treatments. Frequency dependence (or Power-law factor) of storage modulus at low frequency (*S*-LF: 0.584 – 0.784) was higher than at high frequency (*S*-HF: 0.460 – 0.488) and the *S*-LF declined from 0.723±0.074 to 0.584±0.062 with incremental FTC treatments, while FrS and control samples had no significant differences (Table S2). Similar findings of high frequency dependence of G' modulus for refrigerated and frozen low-fat soft cheese has been reported by Meza, et al. (2011). Also, no change was reported in the frequency dependence (0.633 – 0.668) of the G'

values of control and quiescent frozen stored (-20°C, 1-3 months) LMPS Mozzarella cheese, tested at 60°C (Diefes, Rizvi, & Bartsch, 1993).

For both G' and G" values, no significant differences in frequency-dependence were observed at HF for any applied freezing treatments; while frequency-dependency for both G' and G" significantly ($p< 0.05$) reduced with progressive freeze-thaw treatments at LF. Thus, at a low frequency of strain application, calculation of frequency-dependency of either G' or G" could serve as a useful indicator to evaluate whether or not the frozen stored cheese matrix had been exposed to rapid and large scale temperature abuse.

3.4 Measurement of viscoelastic properties using LAOS rheology

3.4.1 Intracycle moduli, shear thinning and strain stiffening behaviour of cheese as affected by freezing treatments

The plot for intracycle large (G'_L) and minimum (G'_M) strain moduli versus strain (0.196-360%) indicated a strong strain-dependent decline for all the treatments (Fig. 3a, 3c). In comparison with the control samples, FTC samples had a lower average values for both the moduli throughout the strain range. Also, the rate of loss of G'_L and G'_M for FTC samples were maximum during transitioning at lower γ values (0.1-1%), which indicates initiation of the breakdown of intact protein network in cheese. However, the FrS samples showed a lower rate of decline in G'_L and G'_M in this region as compared to FTC samples and a continued plateauing (minimum rate of intracycle decline) of moduli was observed in the region $0.1< \gamma <10\%$. This indicates a lower residual intact casein matrix structure in FrS samples in the SAOS region as compared with control and FTC samples. The strain sweep test during LAOS analysis (Fig. 3f; Fig. S4) also confirmed the lowest G' and G" values for FrS samples near transitioning of the SAOS region, complimenting the observations under SAOS (Fig. 2a, 2b) test conditions that

the duration of frozen storage causes more loss in the G' and G" values to the cheese matrix than rapid temperature fluctuations.

The plateauing of G'_L and G'_M values (Fig. 3a, 3c) were also observed in FTC samples in the strain range 1-10%. Plateauing of the moduli could be due to the dynamics of simultaneous bond breaking and bond formations (due to emergence of new binding sites, and thus new hydrogen bonding and hydrophobic interactions) in the proteolysed caseins (as the temperature of analysis remained at 55°C). Also, as the applied strain range is relatively moderate (<10%), large scale irreversible disruption in matrix might not have occurred. Such intermediate changes, especially the formation of transient inter protein linkages upon supply of thermal energy have been reported in cheese matrices (Sharma, et al., 2016) as they are categorised as weak physical gels (Lucey, et al., 2003). At γ >1%, the intracycle moduli for FrS samples (Fig. 3a, 3c) exhibited near complete congruence with the control samples, which could be due to the formation of new bonds within and between aggregated proteins, involving a limited re-association of calcium from the soluble phase (see section 3.3.2).

For all the treatments, plateauing of G'_L and G'_M ended at ~ $\gamma > 10$ and a rapid decline was observed afterwards (Fig. 3a, 3c). This phenomenon is a typical representation of strain transitioning from medium to large strain region, which could abruptly break the residual protein-protein bonds and transient structural gains that may have occurred during the plateauing region. Yildirim-Mavis, Yilmaz, Dertli, Arici, and Ozmen (2019) studied sourdough, where gluten was the principal structure-forming protein, using LAOS; a similar transitioning of intracycle moduli was observed between SAOS to LAOS regions and a region of moderate strain values was referred to as the medium amplitude oscillatory shear (MAOS) region i.e., ~γ=5.2%. However, due to inherent differences between casein and gluten, and the absence of colloidal or soluble calcium in the latter, any plateauing was not observed in the MAOS region. In the present study, the strain range 1< γ <10 % could be considered as the

MAOS region (also the plateauing region) where the rate of decline in the intracycle moduli remains minimal.

The transient network rearrangements during structural collapse could lead to either shear-dependent (Fig. 3b) thickening (T>0) or thinning (T<0) or strain-dependent (Fig. 3d, 3e) structural stiffening (S>0) or softening (S<0). The mathematical background for the above has been given in eq. 11, 12. Intracycle viscosity at large strain-rate (η'_L) and minimum strain-rate (η'_M) also followed a similar declining trend (Fig. S5) as G'_L and G'_M for the range of applied strain; however, the magnitude of intracycle differences between η'_L and η'_M were low as compared to the differences in G'_L and G'_M. This reflected a more strain-stiffening behaviour (Fig. 3d, 3e) at large deformations (γ>10%), as well as transient shear-thickening at γ ~100% (FTC and control samples) and shear-thinning beyond ~ γ >100% (in all samples, Fig.3b). Similar results were reported for cream cheese, where a prominent strain-stiffening and significant shear-thinning were observed at γ>10% (Q. Wang, Espert, Hernández, Salvador, & Sanz, 2024), indicating the complex non-linear rheological transitions exhibited by cheeses at higher deformations. The difference between G'_L and G'_M or η'_L and η'_M remained ~ 0 until the end of the MAOS region (Fig. 3b, 3d), which suggests that, at low to moderate strain values, disruptive intracycle changes in protein-protein interaction does not occur, irrespective of freezing treatments applied.

However, beyond the MAOS region (γ >10%), prominent strain-stiffening (S>0) and comparatively less intense shear-thinning (T<0) behaviour was observed for all the treatments. The rate of stiffening was higher at γ >100 % than at 10< γ <100 % (Fig. 3d, 3e). Higher oscillatory strain amplitude might induce a directional pattern of displacement and physical alignments in the aggregated, softened casein-fat matrix (temperature of analysis 55°C), which could promote faster expulsion of melted fat from the matrix, thereby minimizing the lubrication in the rearranged protein network. Shear-thinning (T<0) behaviour (Fig. 3b), i.e., a

reduction in intracycle dynamic viscosity at γ >100% also compliments this observation. Similar findings were also reported at high strain and temperatures for Kasher cheese, a semi-hard cheese variety (Yildirim-Mavis, et al., 2022).

The FrS samples exhibited lowest strain-stiffening and highest shear-thinning behaviour (Fig. 3b, 3d, 3e) as compared to FTC or control samples (at γ >100%). This could be due to less expulsion of liquid fat from the matrix, possibly due to an increase in residual crystalline fat content as a result of polymorphic changes in fats during prolonged frozen storage (Buldo, et al., 2013). Minor shear-thickening (Fig. 3b) in control and FTC samples at γ ~100 % followed by rapid shear-thinning in all the treatments at γ >100% indicates a sequential interplay of partial protein-hydration, followed by rapid fat expulsion from the matrix at higher strains, as discussed before.

3.4.2 Evaluation of normalised non-linear rheological responses using elastic and viscous Lissajous-Bowditch plots

The aged Gouda cheese (FrS, FTC, and control) in this study were subjected to 26 shear strain values in increasing order from 0.196 to 360% and the stress responses were recorded to calculate different non-linear rheological parameters. Normalized intracycle stress responses (σ/σ_o) were plotted against normalised strain (γ/γ_o) and strain-rate ($\dot{\gamma}/\dot{\gamma}_o$) to obtain elastic and viscous Lissajous-Bowditch (LB) plots, respectively. Elastic and viscous LB plots at different strain values on x-axis and freezing treatments on y-axis were plotted as Pipkin diagrams (Fig. 4). To account for the visual transition of viscoelastic response from SAOS, MAOS and LAOS regions, 5 pertinent strain values i.e., 0.196, 1.19, 59.3, 197, and 360% were selected, representing every region.

For all the treatments, at strain values of 0.196 and 1.19% on an elastic LB plot (Fig. 4a), an elliptical shape with short minor axis indicates the viscoelastic solid characteristics of the matrix, a typical response in close proximity to the SAOS region, although the applied frequency (10 rad/s) was higher than used for SAOS. Within the treatments at low strain values (0.196-1.19%), minor increase in the area (Fig. 4a) of ellipse for FrS and FTC samples (FrS> FTC) are indicative of energy dissipated by the matrix at these strain values, which confirms a greater loss of elastic characteristics in FrS samples than FTC samples. However, as γ progresses >1.19%, the viscoelastic response undertakes an elliptical shape with increasing minor axis and, at γ >59.3%, a rectilinear shape appeared with increasing area under the curve, indicative of a transition to dominant viscoelastic-liquid characteristics (Ewoldt, 2013). A concomitant change in the profile of viscous LB plots can be observed (Fig. 4b) where the broader elliptical shapes at low strain values indicates more solid-like characteristics (0.196< γ<1.19%) and, as strain progresses (> 59.3%), narrow ellipses with short minor axis are linked to a viscoelastic-liquid response of the material. The area under the ellipse on viscous LB plots is indicative of energy stored by the material (Joyner, 2019) and a decline in the area at γ >59.3% compliments the finding of an elastic LB response.

Distortion and rotation of the rectilinear shapes on elastic LB plots started to appear at $\gamma > 100\%$ (plots only shown for 197% and 360%). While the distortion was dominant at high strain values ($\gamma = 197\%$), rotation of curve was dominant at extremely high strains ($\gamma = 360\%$). At very large strains, the disruption of residual protein-protein bonds is almost complete and macroscopic oscillation of structural alignment at large oscillatory strain and harmonic shifts in some structural elements during increasing cycles of freezing-thawing treatments might lead to the rotation of shapes rather than distortion. Also, the rectilinear shapes for control and FrS samples are qualitatively similar; however, for FTC treatments, more rotational changes were observed at higher strain values (γ >197%) than FrS, which further consolidates the evidence

of structural shifts during freeze-thawing cycles. Ewoldt, et al. (2008) reported that clockwise and counter-clockwise rotation of ellipses on an elastic-LB plot relates to strain-stiffening and softening of material, respectively. From quantitative analysis (eq. 11) and qualitative observation of the rotations, the strain-stiffening ratio was found to increase for all the treatments in this study at $\gamma > 100\%$; however, a trend in the order of control >FTC (1-5) >FrS suggests that rapid freezing-thawing, as well as frozen storage, alters the physical environment within which protein, fat, and moisture interacts. But the lowest value for FrS could be a result of increased polymorphic crystallization of the fat phase during prolonged frozen storage (observed through Raman spectroscopic analysis in wavenumber region 3000-2800 cm^{-1}; data not shown), resulting in lesser fat expulsion from the matrix as compared to FTC and control. Similar rotation, rather than deformation, of shapes on elastic LB plots were reported for Mozzarella cheese at higher strain values (~1000 %) and temperatures (10-80°C) by Dahl, et al. (2024).

The secondary loops in elliptical shapes on viscous LB plots were observed at higher strain-rate (γ >197%) for all the treatments with varying magnitude (secondary loop in FrS sample shown in Fig. 5). Ewoldt and McKinley (2010) presented a mathematical interpretation of this as a repetition of the stress response of the material at a given strain-rate. This supports observations of shear-thinning behaviour at intracycle higher strain values and indicates time-dependent shear-thinning or thixotropic behaviour of aged Gouda cheese. However, the variations within the FTC samples for secondary loops were visibly higher than for FrS and control samples at $\gamma = 360\%$. Such results indicate heterogeneity induced in the matrix due to rapid freeze-thawing treatments, which might create localised zones of varying yield and flow behaviours within the cheese matrix due to repeated thermal stress. Here, any possibility of rheological artefacts due to sample preparation and during the analysis could safely be ruled out due to uniformity in sampling process and the use of cross-hatched parallel plate geometry,

654 which virtually eliminates any wall-slips (Dahl, et al., 2024). The observation of a secondary
655 loop at higher strain values (Fig. 4b) for all the treatments is indicative of strong non-linearity
656 in the elastic behaviour of the samples (Hyun, et al., 2011). Similar secondary loops at higher
657 strain-rate have been observed in materials like polystyrene solutions, tomato paste, and guar-
658 gum based solutions (Joyner, 2019). The presence of secondary loops in stress-strain plots
659 represents strong non-linearity in the viscous behaviour of the material (Ewoldt, et al., 2010).

660

661 **3.4.3 Similarity maps for Lissajous-Bowditch plots**

662 Similarity mapping of elastic and viscous responses obtained on respective LB curves is
663 shown in Figure 6. The VAOS tool enables comparing the relative positions of elastic or
664 viscous responses of samples at various strain values from a perfectly elastic or viscous
665 reference points (Dahl, et al., 2024). The approximate linear distance from the reference points
666 is indicated (Fig.6a, 6b) as D_γ and d_γ at various γ values on elastic and viscous similarity maps,
667 respectively. In the elastic similarity map (Fig. 6a), the stress responses at very low strain
668 (0.196-1.19 %) values indicated closest proximity to perfect elastic reference point and, as the
669 strain value increased (59.3, 197 and 360%), the approximate distance of grouped responses
670 increased as well, which indicated strain-dependent evolution of viscoelastic liquid behaviour.
671 Also, the relative positional distribution within the treatments at low to moderate strain values
672 (γ <59.3%) were very narrow, which indicated that FTC and FrS samples generated similar
673 stress responses in the strain range close to LVR regions, although the exact position with
674 respect to the reference point showed minor variations, and these variation in mechanical
675 responses have been successfully quantified in terms of G' and G" using SAOS analysis.

676 At moderate strain value (59.3%), $D_{59.3}$ increased, which indicates that the loss of elastic
677 properties is more due to increased % strain rather than freezing treatments as, within the

treatments, variations were still minimum. However, at higher strain values ($\gamma > 100\%$; only 197 and 360 % have been indicated), a broader spread within the treatment groups were observed. This was evident from the differences in the trend for strain-stiffening and shear-thinning values of FrS, FTC and control samples at $\gamma >$100%. Thus, the impact of freezing on semi-hard cheeses could be more prominently observed during practical deformation scenarios like cutting, shredding, grating, stretching, and chewing. Since the LAOS analysis in this study was limited to 55°C, which is close to the obtained cross-over temperature (53.2±1.6°C), the results are indicative of the performance of semi-hard cheese at large strains with completely melted fat inside the matrix. As discussed in previous sections, that un-melted fat phase could actually mask the real impact of freezing on the structural strength of the protein network.

3.4.4 Evaluation of rheological non-linearity using un-normalised Lissajous-Bowditch plots

Normalisation of stress-strain values provides useful visual qualitative information regarding rheological evolutions in samples; however, it may mask quantitative differences in the deformation behaviour of samples (Dahl, et al., 2024; Yildirim-Mavis, et al., 2019). Hence, un-normalised stress vs. strain and stress vs. strain-rate as 2D-layover strain plots at five different strain values (0.196, 1.19, 59.3, 197, and 360%) for control, FTC5 and FrS samples are presented in Figure 7. Also, a representation of elastic and viscous components of cumulative stress responses at two strain levels (low- 0.196% and high- 360%) is indicated as un-normalised 3D elastic and viscous Lissajous-Bowditch plots (Fig. 8). Both the size and distortion of elliptical shapes (Fig. 7) increased with % strain, but qualitative and quantitative variability at 0.196 and 1.19% strains (see color coding) could not be detected due to the minuscule elliptical projection of elastic and viscous stress responses. This aligns with the

previous observation that freezing has a limited impact on rheological attributes at deformation scale and rates irrelevant to practical applications. Even at moderate strain values ($\gamma \leq 59.3\%$), viscoelasticity dominates irrespective of freezing treatments applied, which is apparent from the enlarging but not distorting elliptical shaped stress-strain response. Such responses are typical of pseudo-linearity shown by cheese matrices (Piñeiro-Lago, et al., 2023), which could be due to the formation of transient structures (see section 3.4.1) during low to moderate controlled strain application.

These temporary protein/peptide bonds are dependent on factors like ripening stage, calcium content distribution, and protein-fat ratio, as well as extrinsic factors like temperature and time scale of rheological measurements (Fox & McSweeney, 1996). However, for $\gamma \geq 59.3\%$, horizontal comparisons within the treatment groups reveal qualitative changes in elastic and viscous responses. Also, the increased distortion of ellipse is concomitant with the loss of elasticity in all the treatments but the distortion in FrS and FTC samples were higher at $\gamma = 360\%$. This is consistent with the observation that freezing has a perceptible impact on the cheese matrix in practical deformation scenarios, as previously discussed.

The stress responses on 3D-stress vs. strain and strain-rate plots indicated minor distortional and rotational variations (Fig. 8) within FTC samples at low strain, i.e., 0.196%. The distortion in the ellipse is perceivable starting from first freeze-thaw cycle when compared with the control samples, and the shape and orientation of ellipse remained almost unchanged for increasing FTC treatments; the lack of significant differences in G' and G" modulus (Table 1) within the FTC treatments (except for the G' of FTC1 sample at 30°C; $p<0.05$) supports this observation. Thus, rapid freeze-thawing leads to microstructural shifts that cause minor rheological differences. Moreover, these microscale differences in FTC samples were not as prominent as the differences quantified for frozen stored samples. At higher strain (360%), distortion in the elliptical stress responses increased for all the samples, in line with the loss in

viscoelasticity. Application of freeze-thawing cycles (1-5 cycles) on caprine milk cheese with low protein (~15%) and high moisture (48%) content was reported to greatly damage the cheese texture (X. Wang, Li, & Zhao, 2023), but the contrasting compositional and ripening differences with the cheese matrix used in the present study does not allow clear comparison of the results. The higher resistance to rapid freeze-thaw cycles in semi-hard matrices could be due to low moisture content which, in turns, results in less expansion during freezing. Also, the high protein content in cheese matrix reduces freezable water content (as more water is bound to caseins) and results in closer packing of the network; thus, increased resistance to structural damage due to ice crystallization could be assumed.

4. Conclusions

Application of small and large amplitude oscillatory shear rheology was found to compliment the broader understanding of freeze-induced structural changes in semi-hard Gouda cheese. SAOS analysis showed that both FTC and FrS type treatments caused loss of structural strength within the protein-fat matrix, but the loss was higher in frozen stored samples. The calculation of activation energy of flow at or above temperatures ensuring complete liquefaction fat could give better information on the effects of freezing on the protein matrix. In the present study, longer frozen storage caused an increase in activation energy of flow at higher temperatures, indicating increased fat crystallization, dehydration and stiffening of the protein matrix. The strain-stiffening (*S*) and shear-thinning (*T*) ratios, calculated using intracycle moduli (G_L', G_M', η_L' and η_M') obtained from LAOS analysis, quantified the impact of freeze-thawing or frozen storage of a semi-hard cheese matrix pertinent to practical deformation situations. Microstructural observations also aligned with these findings. Although the application of multiple freeze-thawing in the present study was intended to

exaggerate the situation of temperature fluctuations, in practical scenarios, however, the temperature abuse would not normally match this scale. Hence, from a rheological perspective, it was observed that semi-hard matrices are fairly inert to short and rapid temperature deviations (relevant to practical conditions). Elastic and viscous Lissajous-Bowditch plots and similarity mapping presented a complete rheological fingerprinting of the semi-hard cheese matrix, as affected by freezing treatments. Similar studies on other cheese types of different ripening status and composition could provide broader understanding of freezing-induced changes relevant to practical application conditions.

Acknowledgements

Digvijay is a recipient of a Walsh Scholarship from Teagasc, the Irish Agricultural and Food Development Authority (Ref 2022059). We thank FrieslandCampina Netherlands for providing the Gouda cheese samples.

Declaration of competing interest

The authors declare that they have no known competing financial interests to influence the work reported in this paper.

References

Alinovi, M., Corredig, M., Mucchetti, G., & Carini, E. (2020). Water status and dynamics of high-moisture Mozzarella cheese as affected by frozen and refrigerated storage. *Food Research International, 137*, 109415.

Alinovi, M., & Mucchetti, G. (2020). Effect of freezing and thawing processes on high-moisture Mozzarella cheese rheological and physical properties. *Lwt, 124*, 109137.

776 Alinovi, M., Mucchetti, G., Wiking, L., & Corredig, M. (2021). Freezing as a solution to preserve the
777 quality of dairy products: The case of milk, curds and cheese. *Critical Reviews in Food Science*
778 *and Nutrition, 61*(20), 3340-3360.
779 Alvarenga, N., & Sousa, I. (2011). Effect of freezing on the rheological, chemical and colour properties
780 of Serpa cheese. *Journal of dairy research, 78*(1), 80-87.
781 Berg, G. v. d., & Koning, P. d. (1990). Gouda cheesemaking with purified calf chymosin and microbially
782 produced chymosin.
783 Bertola, N., Califano, A., Bevilacqua, A., & Zaritzky, N. (1996). Effect of freezing conditions on functional
784 properties of low moisture Mozzarella cheese. *Journal of Dairy Science, 79*(2), 185-190.
785 Buaynov, O., & Buaynova, I. (2016). The physical and chemical changes of water and the hydration of
786 the protein complex in cheese during freezing. *Foods and Raw materials, 4*(1), 13-18.
787 Buldo, P., Andersen, U., & Wiking, L. (2013). Microstructure and material properties of milk fat systems
788 during temperature fluctuations. *Food Biophysics, 8*, 262-272.
789 Cho, K. S., Hyun, K., Ahn, K. H., & Lee, S. J. (2005). A geometrical interpretation of large amplitude
790 oscillatory shear response. *Journal of Rheology, 49*(3), 747-758.
791 Dahl, J. F., Gregersen, S. B., Andersen, U., Schulz, H.-J., & Corredig, M. (2024). Small and large
792 deformation rheology on pizza cheese as an example of application to study anisotropic
793 properties of food soft materials. *Food Hydrocolloids, 148*, 109456.
794 Diefes, H. A., Rizvi, S., & Bartsch, J. (1993). Rheological behavior of frozen and thawed low-moisture,
795 part-skim Mozzarella cheese. *Journal of Food Science, 58*(4), 764-769.
796 Digvijay, Kelly, A. L., & Lamichhane, P. (2023). Ice crystallization and structural changes in cheese
797 during freezing and frozen storage: implications for functional properties. *Critical Reviews in*
798 *Food Science and Nutrition*, 1-24.
799 Ewoldt, R. H. (2013). Defining nonlinear rheological material functions for oscillatory shear. *Journal of*
800 *Rheology, 57*(1), 177-195.
801 Ewoldt, R. H., Clasen, C., Hosoi, A. E., & McKinley, G. H. (2007). Rheological fingerprinting of gastropod
802 pedal mucus and synthetic complex fluids for biomimicking adhesive locomotion. *Soft Matter,*
803 *3*(5), 634-643.
804 Ewoldt, R. H., Hosoi, A., & McKinley, G. H. (2008). New measures for characterizing nonlinear
805 viscoelasticity in large amplitude oscillatory shear. *Journal of Rheology, 52*(6), 1427-1458.
806 Ewoldt, R. H., & McKinley, G. H. (2010). On secondary loops in LAOS via self-intersection of Lissajous–
807 Bowditch curves. *Rheologica acta, 49*, 213-219.
808 Faber, T., Van Breemen, L., & McKinley, G. (2017). From firm to fluid–Structure-texture relations of
809 filled gels probed under Large Amplitude Oscillatory Shear. *Journal of Food Engineering, 210*,
810 1-18.
811 Famelart, M.-H., Le Graet, Y., & Raulot, K. (1999). Casein micelle dispersions into water, NaCl and
812 CaCl2: physicochemical characteristics of micelles and rennet coagulation. *International Dairy*
813 *Journal, 9*(3-6), 293-297.
814 Fennema, O. (1972). Freezing of cheese-pros and cons. *Western milk ice cream news, 20*.
815 Fontecha, J., Kaláb, M., Medina, J. A., Peláez, C., & Juárez, M. (1996). Effects of freezing and frozen
816 storage on the microstructure and texture of ewe's milk cheese. *Zeitschrift für Lebensmittel-*
817 *Untersuchung und Forschung, 203*, 245-251.
818 Fox, P., & McSweeney, P. (1996). Proteolysis in cheese during ripening. *Food Reviews International,*
819 *12*(4), 457-509.
820 Gelder, K. v. (2023). Value of the import and export of Gouda cheese in the Netherlands 2008-2021.
821 In (Vol. 2024): Statista.
822 Guinee, T. P., & Fox, P. F. (2017). Salt in cheese: physical, chemical and biological aspects. In *Cheese*
823 (pp. 317-375): Elsevier.
824 Huppertz, T., Gazi, I., Luyten, H., Nieuwenhuijse, H., Alting, A., & Schokker, E. (2017). Hydration of
825 casein micelles and caseinates: Implications for casein micelle structure. *International Dairy*
826 *Journal, 74*, 1-11.

827 Hyun, K., Wilhelm, M., Klein, C. O., Cho, K. S., Nam, J. G., Ahn, K. H., Lee, S. J., Ewoldt, R. H., & McKinley,
828 G. H. (2011). A review of nonlinear oscillatory shear tests: Analysis and application of large
829 amplitude oscillatory shear (LAOS). *Progress in polymer science, 36*(12), 1697-1753.
830 Johnston, D. (2000). The effects of freezing at high pressure on the rheology of Cheddar and
831 Mozzarella cheeses. *Milchwissenschaft, 55*(10), 559-562.
832 Joyner, H. S. (2019). *Rheology of semisolid foods*: Springer.
833 Kasprzak, K., Wendorff, W., & Chen, C. (1994). Freezing qualities of Cheddar-type cheeses containing
834 varied percentages of fat, moisture, and salt. *Journal of Dairy Science, 77*(7), 1771-1782.
835 Kuo, M.-I., & Gunasekaran, S. (2003). Effect of frozen storage on physical properties of pasta filata and
836 nonpasta filata Mozzarella cheeses. *Journal of Dairy Science, 86*(4), 1108-1117.
837 Kuo, M.-I., & Gunasekaran, S. (2009). Effect of freezing and frozen storage on microstructure of
838 Mozzarella and pizza cheeses. *LWT-Food Science and Technology, 42*(1), 9-16.
839 Lamichhane, P., Kelly, A. L., & Sheehan, J. J. (2018). Symposium review: Structure-function
840 relationships in cheese. *Journal of Dairy Science, 101*(3), 2692-2709.
841 Lamichhane, P., Sharma, P., Kennedy, D., Kelly, A. L., & Sheehan, J. J. (2019). Microstructure and
842 fracture properties of semi-hard cheese: Differentiating the effects of primary proteolysis and
843 calcium solubilization. *Food Research International, 125*, 108525.
844 Läuger, J., & Stettin, H. (2010). Differences between stress and strain control in the non-linear behavior
845 of complex fluids. *Rheologica acta, 49*(9), 909-930.
846 Lucey, J., Johnson, M., & Horne, D. (2003). Invited review: Perspectives on the basis of the rheology
847 and texture properties of cheese. *Journal of Dairy Science, 86*(9), 2725-2743.
848 Madsen, J., Sode, L., Dahl, J. F., Corredig, M., & Schulz, H.-J. (2022). Visual Exploration of Rheological
849 Test Results from Soft Materials. In *2022 First International Workshop on Visualization in*
850 *Testing of Hardware, Software, and Manufacturing (TestVis)* (pp. 1-7): IEEE.
851 McMahon, D. J., & Oberg, C. J. (2017). Pasta-filata cheeses. In *Cheese* (pp. 1041-1068): Elsevier.
852 Melito, H., Daubert, C., & Foegeding, E. (2013). Relationships between nonlinear viscoelastic behavior
853 and rheological, sensory and oral processing behavior of commercial cheese. *Journal of*
854 *Texture Studies, 44*(4), 253-288.
855 Meza, B. E., Verdini, R. A., & Rubiolo, A. C. (2011). Effect of freezing on the viscoelastic behaviour
856 during the ripening of a commercial low-fat soft cheese. *International Dairy Journal, 21*(5),
857 346-351.
858 Oberg, C. J., Merrill, R. K., Brown, R. J., & Richardson, G. H. (1992). Effects of freezing, thawing, and
859 shredding on low moisture, part-skim Mozzarella cheese. *Journal of Dairy Science, 75*(5), 1161-
860 1166.
861 OECD/FAO. (2021). *OECD-FAO Agricultural*
862 *Outlook 2021-2030*. Paris: OECD Publishing.
863 Page, R. M., Magan, J. B., Mannion, D. T., Kilcawley, K. N., Murphy, J. P., Kennedy, E., O'Donovan, M.,
864 Tobin, J. T., O'Mahony, J. A., & O'Callaghan, T. F. (2024). The impacts of milking frequency on
865 nutrient composition and functional characteristics of Cheddar cheese. *International Journal*
866 *of Dairy Technology, 77*(3), 630-644.
867 Pax, A. P., Ong, L., Pax, R. A., Vongsvivut, J., Tobin, M. J., Kentish, S. E., & Gras, S. L. (2023). Industrial
868 freezing and tempering for optimal functional properties in thawed Mozzarella cheese. *Food*
869 *Chemistry, 405*, 134933.
870 Piñeiro-Lago, L., Ramlawi, N., Franco, I., Tovar, C. A., Campo-Deaño, L., & Ewoldt, R. H. (2023). Large
871 amplitude oscillatory shear stress (LAOStress) analysis for an acid-curd Spanish cheese:
872 Afuega'l Pitu atroncau blancu and roxu (PDO). *Food Hydrocolloids, 142*, 108720.
873 Reid, D. S., & Yan, H. (2004). Rheological, melting and microstructural properties of cheddar and
874 mozzarella cheeses affected by different freezing methods. *Journal of food quality, 27*(6), 436-
875 458.

Ribero, G. G., Rubiolo, A. C., & Zorrilla, S. E. (2009). Microstructure of Mozzarella cheese as affected by the immersion freezing in NaCl solutions and by the frozen storage. *Journal of food engineering, 91*(4), 516-520.
Seighalani, F. Z. B., & Joyner, H. (2019). Wear: A new dimension of food rheological behaviors as demonstrated on two cheese types. *Journal of Food Engineering, 263*, 337-340.
Shahbandeh, M. (2024). Market value of cheese worldwide from 2019 to 2032. In (Vol. 2024, pp. Cheese market value worldwide 2019-2032).
Sharma, P., Munro, P. A., Dessev, T. T., & Wiles, P. G. (2016). Shear work induced changes in the viscoelastic properties of model Mozzarella cheese. *International Dairy Journal, 56*, 108-118.
Sommer, H. (1928). The freezing point of Cheddar cheese: Injury of cheese by freezing. *Journal of Dairy Science, 11*(1), 9-17.
Timlin, M., Brodkorb, A., Harbourne, N., O'Callaghan, T. F., Drouin, G., Pacheco-Pappenheim, S., Hennessy, D., O'Donovan, M., Pierce, K. M., & Corrigan, B. M. (2024). The impact of seasonal calving systems with varying pasture allowance on Cheddar cheese composition, nutritional quality and ripening characteristics. *Journal of Dairy Science*.
To, C. M., Vermeir, L., Rebry, F., Kerkaert, B., Van der Meeren, P., & Guinee, T. P. (2020). Impact of freezing on the physicochemical and functional properties of low–moisture part–skim mozzarella. *International Dairy Journal, 106*, 104704.
Tomaszewska-Gras, J., Cais-Sokolińska, D., Bierzuńska, P., Kaczyński, Ł. K., Walkowiak, K., & Baranowska, H. M. (2019). Behaviour of water in different types of goats' cheese. *International Dairy Journal, 95*, 18-24.
Tunick, M. H. (2010). Activation energy measurements in rheological analysis of cheese. *International Dairy Journal, 20*(10), 680-685.
Tunick, M. H. (2011). Small-strain dynamic rheology of food protein networks. *Journal of agricultural and food chemistry, 59*(5), 1481-1486.
Udyarajan, C. T., Horne, D. S., & Lucey, J. A. (2007). Use of time–temperature superposition to study the rheological properties of cheese during heating and cooling. *International journal of food science & technology, 42*(6), 686-698.
Van Hekken, D., Tunick, M., & Park, Y. (2005). Effect of frozen storage on the proteolytic and rheological properties of soft caprine milk cheese. *Journal of Dairy Science, 88*(6), 1966-1972.
Verdini, R. A., Zorrilla, S., & Rubiolo, A. C. (2005). Effects of the freezing process on proteolysis during the ripening of Port Salut Argentino cheeses. *International Dairy Journal, 15*(4), 363-370.
Wang, Q., Espert, M., Hernández, M., Salvador, A., & Sanz, T. (2024). Effect of cellulose ether emulsion and oleogel as healthy fat alternatives in cream cheese. Linear and nonlinear rheology, texture and sensory properties. *Food Hydrocolloids, 150*, 109740.
Wang, X., Li, Y., & Zhao, Z. (2023). Freezing-induced changes in goat cheese: Effect of freezing rate, storage and freeze–thaw cycles. *International Journal of Dairy Technology, 76*(2), 436-441.
Wiśniewska, K., Grześkiewicz, A., Jankowska, A., & Reps, A. (2012). Feasibility of frozen storage of Gouda cheese.
Yildirim-Mavis, C., Ozmen, D., Yakisik, E., Toker, O. S., Palabiyik, I., & Kaner, O. (2022). Evaluation of kashar cheese meltability by tack and large amplitude oscillatory shear (LAOS) tests. *International Dairy Journal, 127*, 105242.
Yildirim-Mavis, C., Yilmaz, M. T., Dertli, E., Arici, M., & Ozmen, D. (2019). Non-linear rheological (LAOS) behavior of sourdough-based dough. *Food Hydrocolloids, 96*, 481-492.

Figure

Click here to access/download;Figure;3_List of Figures-Gouda- final.docx

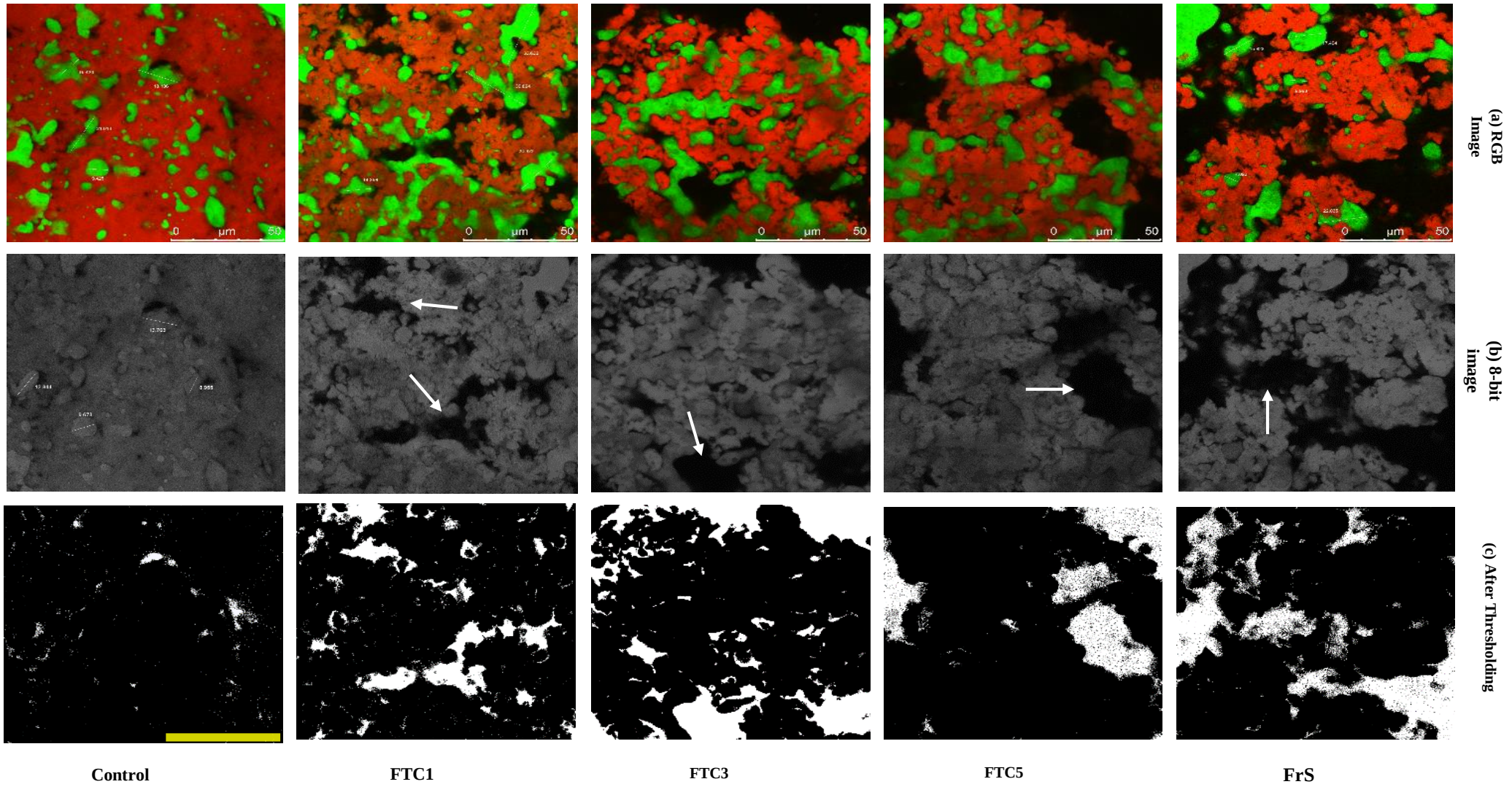


Figure 1. Freezing-induced changes in the microstructure of Gouda cheese. **(a)** Red corresponds to protein and green to fat in RGB images; **(b)** CLSM images converted into 8-bit images, the dark region marked with white arrows indicate empty space created after freeze-thawing and frozen storage treatments, while grey regions indicates combined protein-fat network; **(c)** Segmentation of 8-bit image by thresholding, white regions indicate empty space. Yellow bar is indicative of 50 µm scale length in all micrographs.

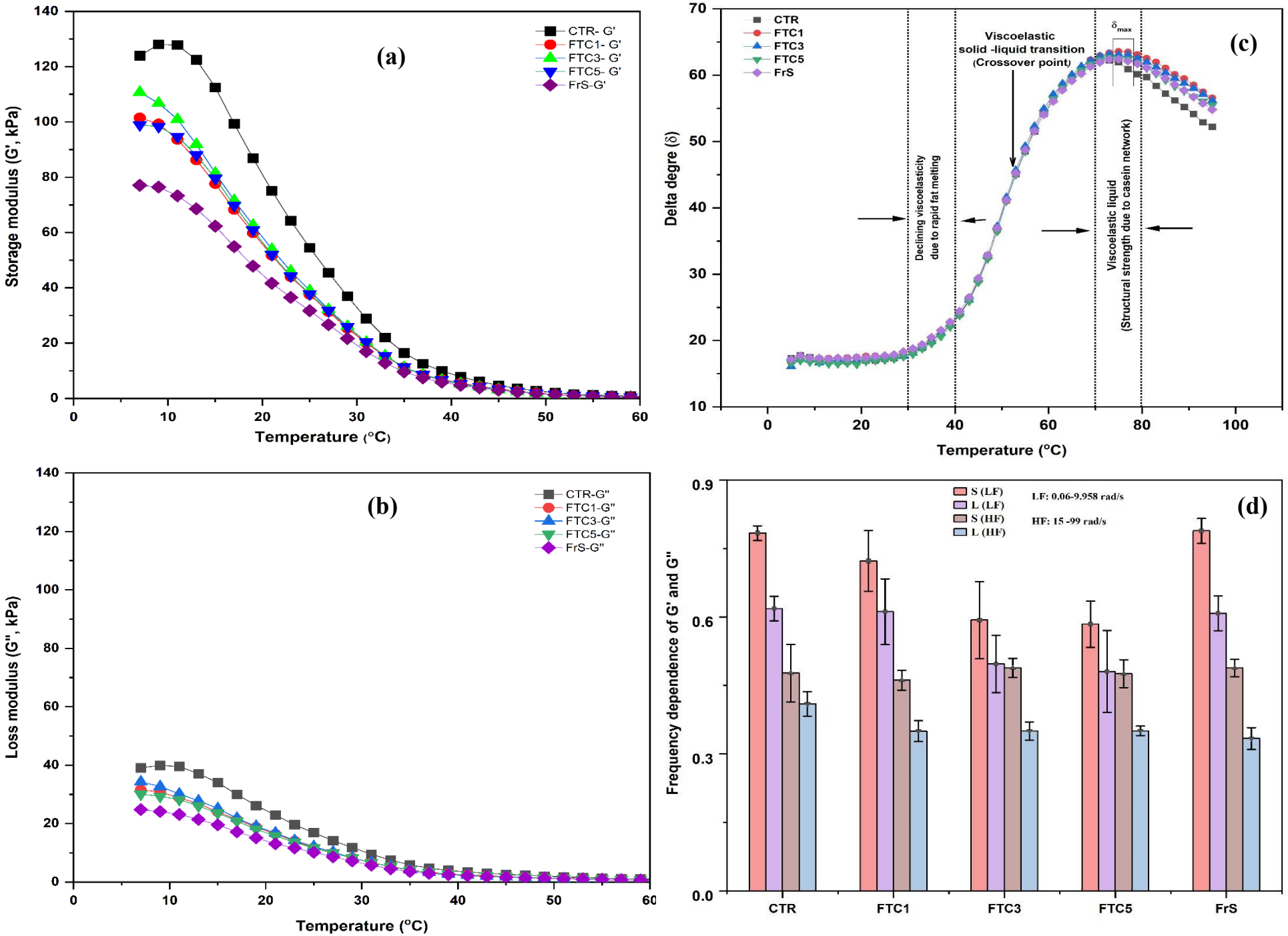


Figure 2. (a) Storage modulus; **(b)** loss modulus; **(C)** delta degree obtained during temperature sweep test, where arrows indicate two temperature zones used for activation energy calculation; **(d)** Frequency dependence of storage (G') and loss modulus (G"), where S- Power-law coefficient for G'; L- Power-law coefficient for G"; LF-Low frequency (0.06-9.958 rad/s); HF- High frequency (15-99 rad/s)

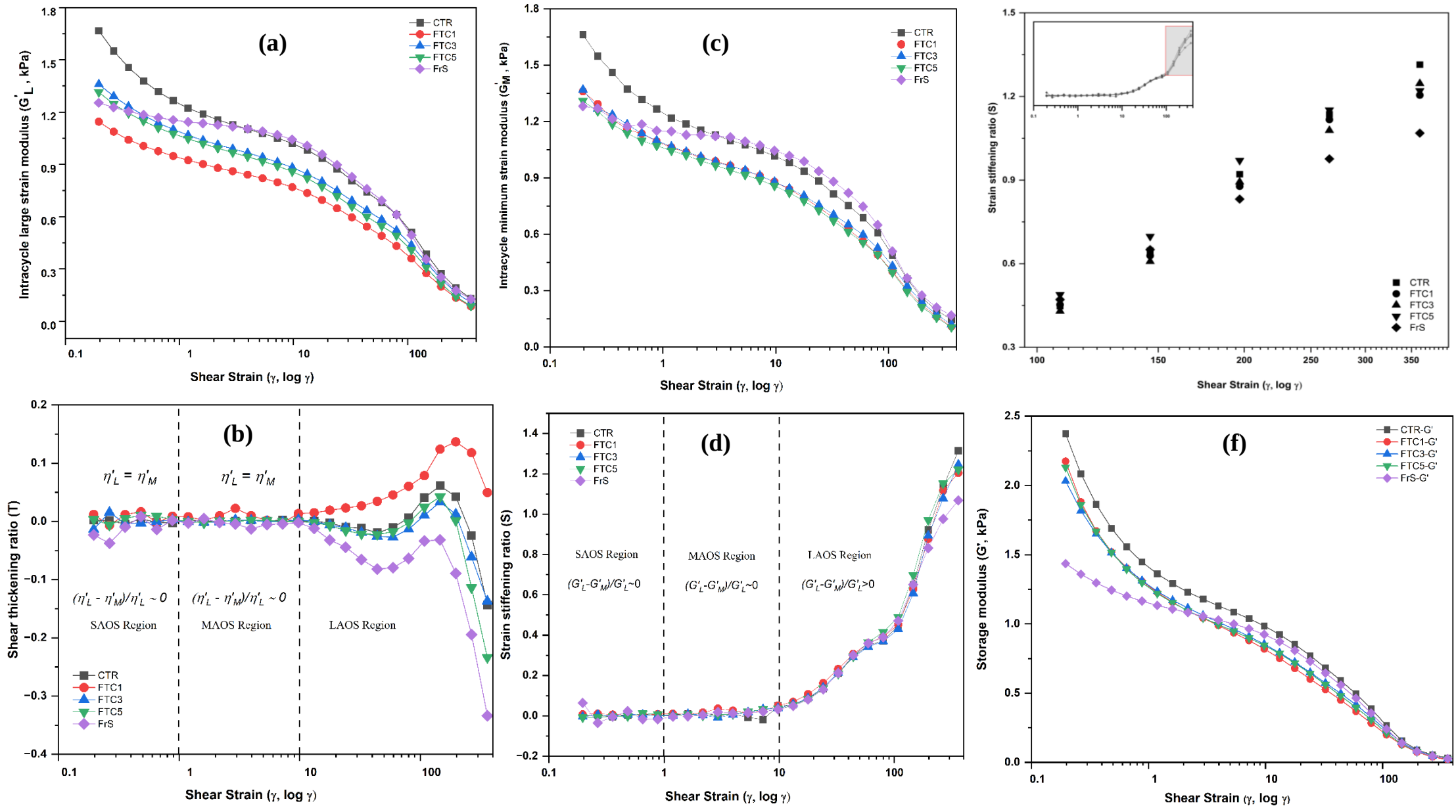


Figure 3. (a) Intracycle large strain (G'_L) modulus; **(b)** Shear thickening (*T*) ratio; **(c)** Intracycle minimum strain (G'_M) modulus; **(d, e)** Strain stiffening (*S*) ratio **(f)** Storage modulus during strain sweep analysis under LAOS test conditions

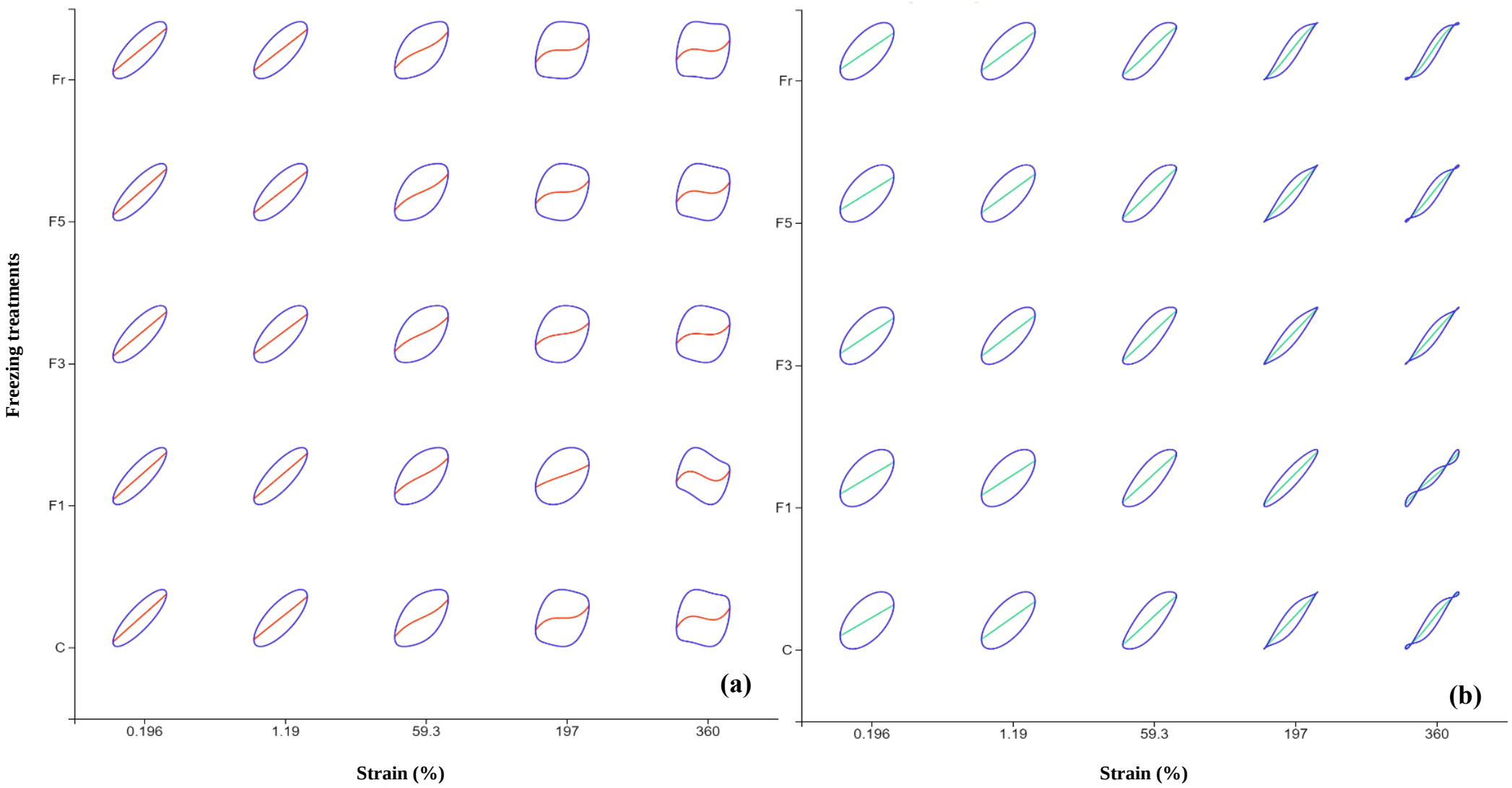


Figure. 4 (a) Stress vs. strain (elastic) Lissajous-Bowditch plots; **(b)** Stress vs. strain rate (viscous) Lissajous-Bowditch plots of Gouda cheese at progressive strain values transitioning from SAOS to LAOS region. C- Control; F1- FTC1; F3- FTC3; F5- FTC5; Fr- FrS

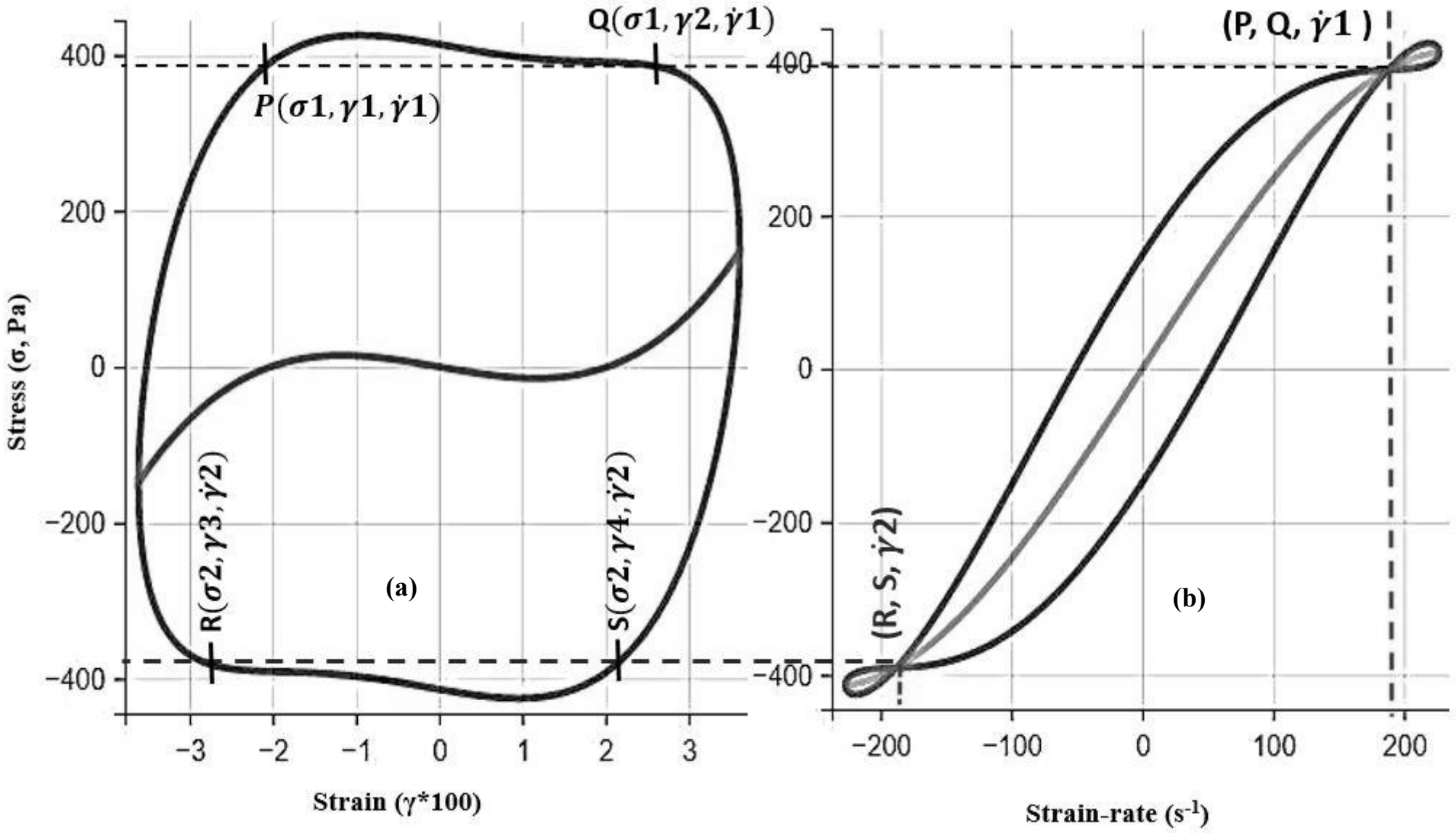


Figure 5. Intracycle repetition of stress responses σ1 and σ2 at strain-rates $\dot{\gamma}1$ and $\dot{\gamma}2$, respectively, observed as secondary looping in un-normalised viscous Lissajous-Bowditch plot **(b)** at high strain value (360%), plotted against elastic Lissajous-Bowditch plot **(a)** at the same strain %. The illustration only indicates secondary looping in frozen stored (FrS) semi-hard cheese.

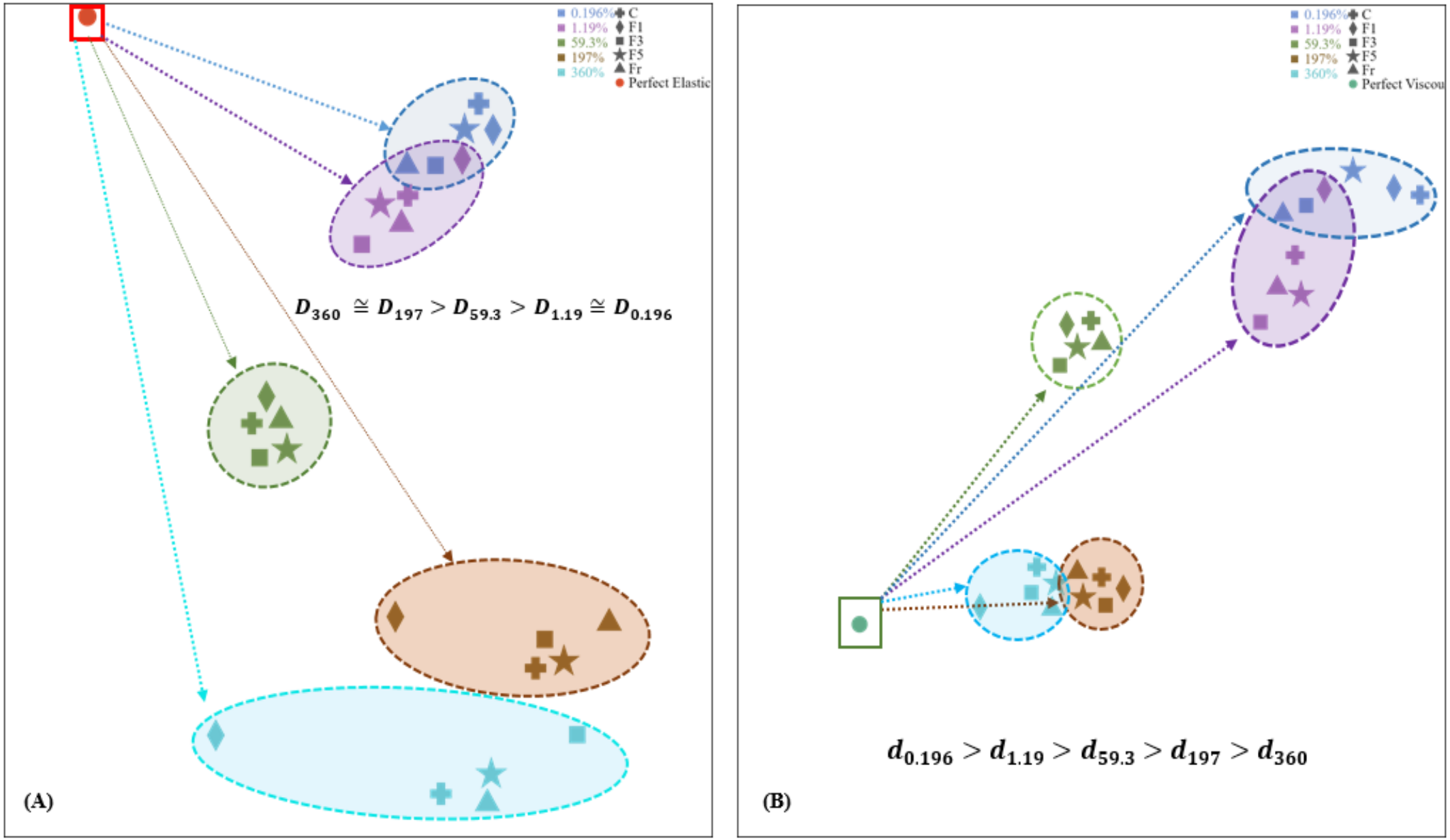


Figure 6. Similarity map; **(a)** from a purely elastic perspective; **(b)** from a purely viscous perspective) based on viscoelastic material response of Gouda cheese as affected by different freezing treatments (C- Control; F1- FTC1; F3- FTC3; F5- FTC5; Fr- FrS). Clusters of responses at same strain values have been shown in color coded loops as a guide for the eye (not to scale). Where D_n and d_n are approximate linear distances of different clusters from perfect elastic and viscous reference points in plot (A) and (B), respectively. Subscript *n* refers to strain (%) value.

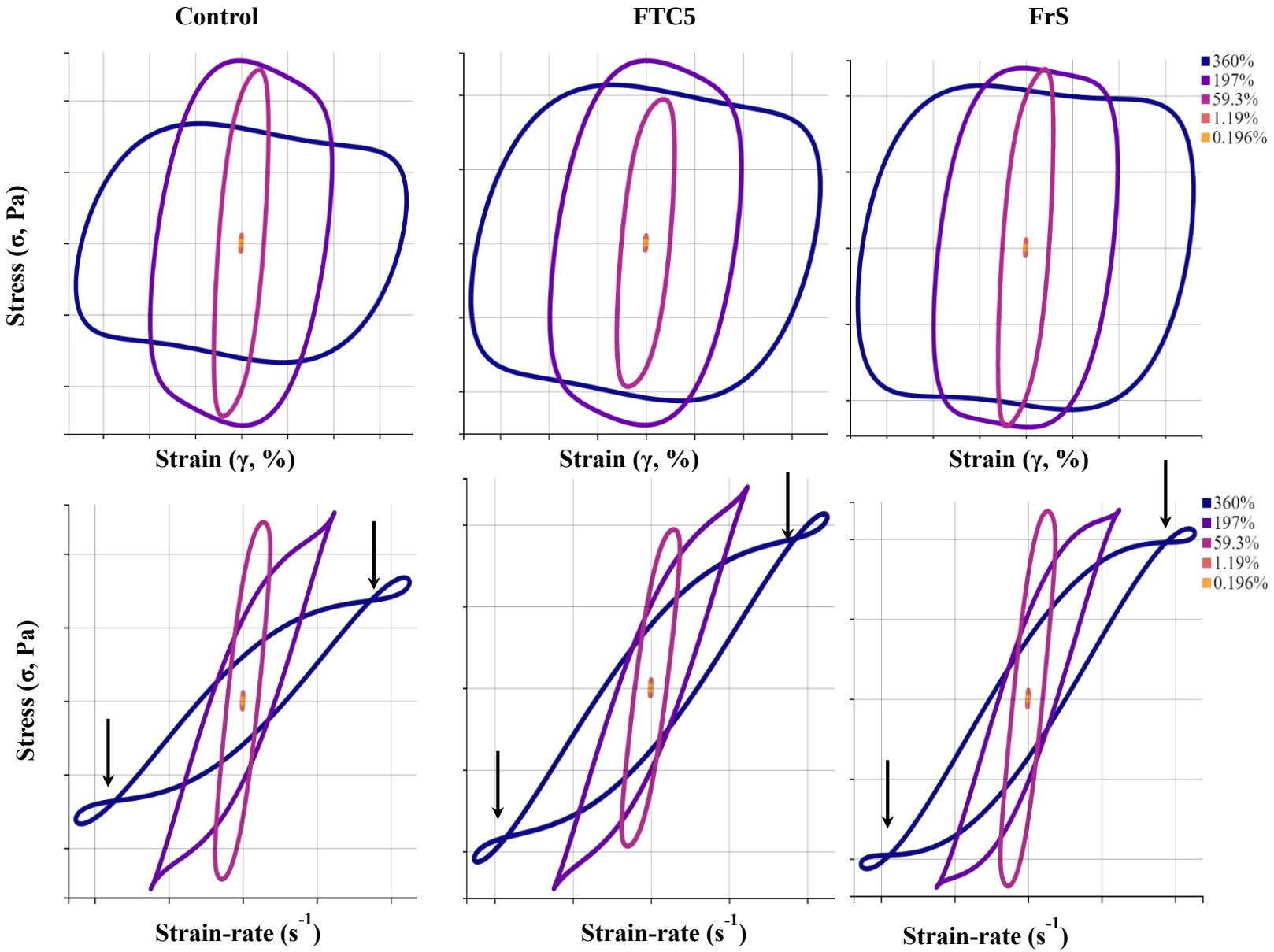


Figure 7. 2D layover strain plots of elastic and viscous Lissajous-Bowditch plots (un-normalised) of the Gouda samples (control, FTC5 and FrS) at different strain values (color coded for different strain %). Arrows in black indicates secondary looping in un-normalised viscous LB plots at higher strain-rate.

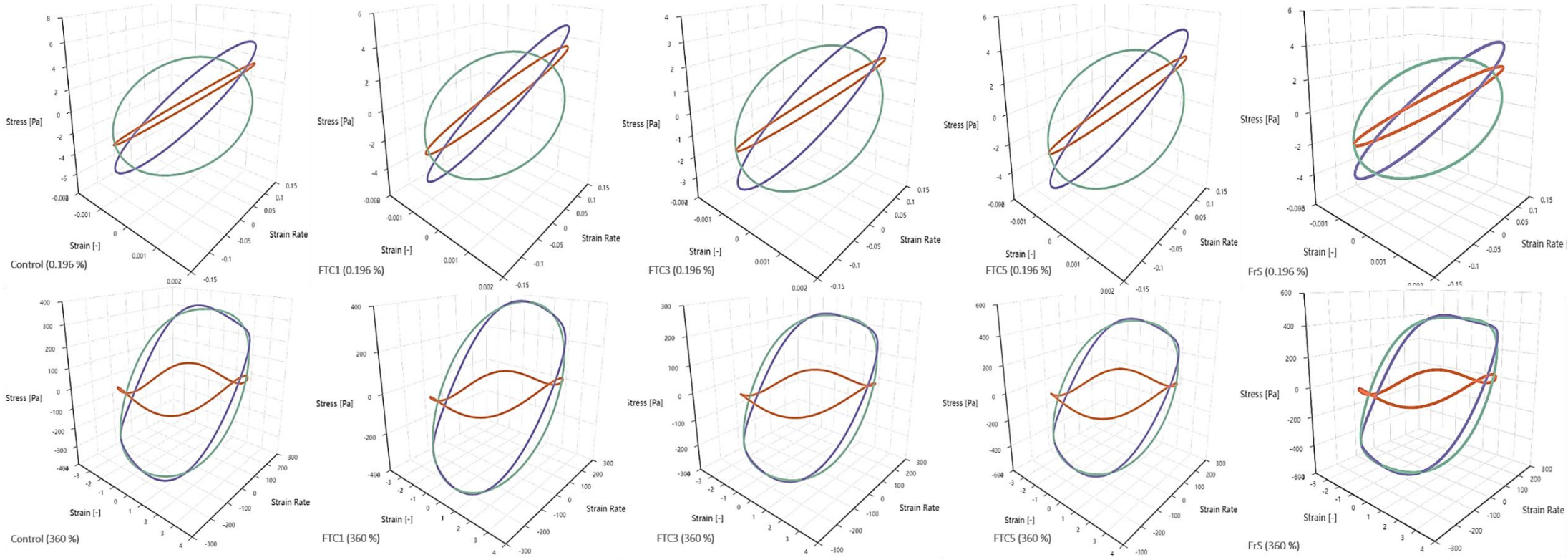


Figure 8. Un-normalised orthogonal stress decomposition of cumulative stress response (in blue) into elastic (red; stress vs. strain plot) and viscous (green; stress vs. strain-rate plot) components at low strain (0.196%, top row) and high strain (360%, bottom row) of a semi-hard cheese matrix subjected to different freezing treatments (Control, FTC1, FTC3, FTC5, FrS; from left to right). Since the projections are not normalised, scale of plot should be noted.

Table (Editable version) Click here to access/download;Table (Editable version);4_List of table-final.docx

Table 1. Storage (G') and loss (G") modulus at different temperatures obtained during a temperature sweep test of cheese samples subjected to different freezing treatments (mean ± standard deviation of three replicate trials).

Treatment	Storage modulus (G', kPa)			Loss modulus (G", kPa)		
	10°C	30°C	50°C	10°C	30°C	50°C
Control	125.55±15.54[a]	36.90±9.29[a]	2.73±0.95[a]	39.99±9.05[a]	11.78±2.86[a]	1.99±0.56[a]
FTC1	99.30±12.79[a]	25.31±2.61[b]	1.97±0.34[a]	30.78±3.86[a]	8.26±0.72[b]	1.45±0.16[a]
FTC3	106.81±14.78[a]	26.08±3.07[a]	1.82±0.05[a]	32.69±4.31[a]	8.28±0.92[b]	1.39±0.09[b]
FTC5	98.32 ±9.32[a]	25.92±8.20[a]	1.89±0.59[a]	29.31±8.41[a]	8.23±2.64[b]	1.40±0.45[b]
FrS	65.28±12.19[b]	19.65±7.32[b]	1.58±0.38[b]	20.27±4.32[b]	5.70±1.39[b]	1.22±0.19[b]

*Means in the same column with different superscripts are significantly different ($P<0.05$)

Table 2. Activation energy of flow in the temperature range 30-40ºC and 70-80ºC, and maximum delta degree (δ_{max}) and crossover temperature (CT) obtained during temperature sweep analysis of cheese samples subjected to different freezing treatments (mean ± standard deviation of three replicate trials).

Treatment	E_a-t (30-40ºC), kJ/mol	E_a-T (70-80ºC), kJ/mol	$T_{\delta\text{-max}}$ (ºC)	Maximum delta (δ_{max}; rad)	Crossover temperature (ºC ; at δ_{45})
Control	103.05±6.95[a]	27.23±2.01[a]	71.67±1.63[a]	62.28±2.87[a]	53.83±0.75[a]
FTC1	100.71±6.08[a]	44.26±3.10[b]	74.67±3.67[a]	63.85±1.71[a]	52.83±2.22[a]
FTC3	106.62±4.05[a]	43.57±4.03[b]	74.44±2.06[a]	63.42±1.33[a]	52.50±1.38[a]
FTC5	104.49±3.07[a]	34.99±1.13[c]	75.01±3.35[a]	62.89±1.20[a]	53.00±1.09[a]
FrS	105.31±5.98[a]	48.29±1.80[b]	74.55±2.34[a]	62.55±1.52[a]	52.17±1.47[a]

*Means in the same column with different superscripts are significantly different (P<0.05)

Declaration of interests

☒ The authors declare that they have no known competing financial interests or personal relationships that could have appeared to influence the work reported in this paper.

☐ The author is an Editorial Board Member/Editor-in-Chief/Associate Editor/Guest Editor for *[Journal name]* and was not involved in the editorial review or the decision to publish this article.

☐ The authors declare the following financial interests/personal relationships which may be considered as potential competing interests:

Author Statement:

The corresponding author confirms that all authors have made substantial contributions to all of the following:

1. The conception and design of the study, or acquisition of data, or analysis and interpretation of data.

2. Drafting the article or revising it critically for important intellectual content.

3. Final approval of the version to be submitted.

All authors agreed to be accountable for all aspects of the work to ensure that the questions related to the accuracy or integrity of any part of the work are appropriately investigated and resolved.

Digvijay: Conceptualization, Data curation, Formal analysis, Investigation, Methodology, Software, Validation, Visualization, Writing – original draft

Thom Huppertz: Resources, Validation, Writing – review & editing

Alan L. Kelly: Conceptualization, Funding acquisition, Project administration, Supervision, Validation, Writing – review & editing

Prabin Lamichhane: Conceptualization, Funding acquisition, Methodology, Project administration, Resources, Supervision, Validation, Writing – review & editing

Click here to access/download
Supplementary Material
5_Supplementary_table-final.docx

Click here to access/download
Supplementary Material
6_Supplementary_figures_final.docx

Characterisation of the impact of freezing on ripened Gouda cheese using small and large amplitude oscillatory shear rheology

Digvijay [a, b], Thom Huppertz[b, c], Alan L. Kelly[b], Prabin Lamichhane[a*]

[a]Teagasc Food Research Center, Moorepark, Fermoy, Co. Cork, Ireland, P61 C996

[b]School of Food and Nutritional Sciences, University College Cork, Ireland, T12 YN60

[c] FrieslandCampina, Stationsplein 4, 3818, LE, Amersfoort, the Netherlands

***Author for correspondence: prabin.lamichhane@teagasc.ie**

Abstract

In this study, small amplitude oscillatory shear rheology (SAOS) and large amplitude oscillatory shear rheology (LAOS) were applied as complementary techniques to map the impact of two different freezing schemes, i.e., multiple rapid freeze-thaw cycles (FTC; -18 ±1 to 6°C) and quiescent frozen storage (FrS; -18 ±1°C, 3-months), on rheological and microstructural properties of aged (9 months) Gouda cheese. The modes of impact of FTC and FrS treatments were different, and LAOS was found to be a powerful tool to quantify such differences at practical deformation scales. The activation energy (Ea) of flow calculated above and below the crossover temperature (53.2±1.6°C) and frequency-dependence of storage (G') modulus were used to quantify freezing-induced thermo-rheological changes in the SAOS region. At large incremental deformations (10-360%), freezing impacted the intracycle elastic (G'_L, G'_M) moduli and intracycle viscous (η'_L, η'_M) moduli, resulting in strain-dependent zones of strain-stiffening and shear-thinning in the cheese matrix. Micro-cracks observed by confocal laser scanning microscopy (CLSM) were consistent with observed changes in the linear and non-linear rheological responses. This study provides a critical understanding of differences in the effects of FTC and FrS-type treatments, pertinent to practical frozen storage scenarios of Gouda cheese and other semi-hard dairy matrices.

1. Introduction

Global cheese production is on the rise, with an estimated growth of around 15% between 2020 to 2030, and is expected to reach a market value of $143 billion by 2032 (OECD/FAO, 2021; Shahbandeh, 2024). This growth is primarily driven by demand from food processors in China and other milk deficit countries in the Southeast Asia and the Middle East. To cater to the global markets, long distance frozen shipping of cheeses from primary producers in Europe and the USA is sometimes carried out to extend its techno-functional (cutting, slicing, shredding, grating, melting) shelf life (To, et al., 2020). Moreover, to address variability in cheese quality due to seasonal milk production systems (Timlin, et al., 2024), frozen storage is often preferred for bulk cheese procurement to provide greater flexibility in the duration of its usage. Also, to handle surplus production stock and stabilise demand-supply fluctuations, freezing may be applied to stop ripening at certain ages (Alinovi, Mucchetti, Wiking, & Corredig, 2021; Digvijay, Kelly, & Lamichhane, 2023).

During frozen storage of cheese, composition and microbial growth remain unchanged; however, texture-functional and overall sensory attributes can be adversely affected, and the extent of the effect varies based on the cheese type and composition (Digvijay, et al., 2023). Freezing causes localized concentration gradient formation, cryo-concentration of soluble components, dehydration of the casein-fat matrix, damage to the matrix due to ice recrystallization, and readjustments in the distribution of moisture and salts, as well as uneven reabsorption of moisture by the casein-fat network upon thawing (Alinovi, et al., 2021; Digvijay, et al., 2023; Meng-I Kuo & Gunasekaran, 2009; Reid & Yan, 2004; Verdini, Zorrilla, & Rubiolo, 2005). However, some prior studies have reported inconclusive results about the changes caused by freezing cheese (Fennema, 1972) and highlighted that the effect of freezing varies based on cheese type, size and rate of freezing used for the study (Oberg, Merrill, Brown,

72 & Richardson, 1992). Hence, cautious application of freezing is recommended for cheeses
73 (Alinovi, et al., 2021; Bertola, Califano, Bevilacqua, & Zaritzky, 1996).

74 Both, low moisture part-skim (LMPS) and high moisture Mozzarella have been
75 extensively investigated under different frozen storage conditions (Pax, et al., 2023; To, et al.,
76 2020). However, the anisotropic nature of Mozzarella cheese restricts the generalization of
77 obtained results to frozen storage of non-pasta filata type cheeses. Cheddar and Gouda-type
78 cheeses are among the highest-selling semi-hard cheeses in the United States and Europe. The
79 Netherlands is the largest exporter of Gouda-type Dutch cheeses, with a trade value of 1.26
80 billion euros in 2021 (Gelder, 2023). There is a growing interest in the prospects of freezing
81 such cheeses at different ripening stages, targeting specific consumer markets and to stabilize
82 supply-chain fluctuations (Alinovi, et al., 2021). Surprisingly, however, only one published
83 report was found on the effects of frozen storage on Gouda cheese regarding its rheology and
84 microstructure (Wiśniewska, Grześkiewicz, Jankowska, & Reps, 2012), and it provided limited
85 information. Also, only a few studies have investigated the impact of freezing and frozen
86 storage on other non-pasta filata type hard and semi-hard cheeses (Johnston, 2000; Kasprzak,
87 Wendorff, & Chen, 1994; Reid, et al., 2004; Sommer, 1928). These studies, moreover, exclude
88 the impacts of temperature fluctuations, which are unavoidable during frozen storage and
89 shipping, on the cheese matrix.

90 Temperature fluctuations at sub-zero temperature conditions results in growth of ice-
91 crystals by Ostwald-ripening, resulting in significant textural and rheological alterations in
92 food and dairy products (Digvijay, et al., 2023). To date, however, critical understanding
93 related to rheological and microstructural properties of semi-hard cheeses as affected by
94 freezing, frozen-storage, and large-scale temperature fluctuations is limited. Hence, to address
95 these research gaps, aged Gouda cheese (ripened for 9 months) was selected as a model semi-

hard matrix for the freezing study as it presented a unique consistency. The results can also help in understanding the effects of freezing on similar semi-hard dairy matrices.

In most of the published literature (Alinovi & Mucchetti, 2020; Alvarenga & Sousa, 2011; Meza, Verdini, & Rubiolo, 2011), SAOS analysis has been used to study the rheological characteristics of frozen-thawed cheeses, restricting the applied shear strain (γ) within the critical strain (γ_c) limit of the viscoelastic region (LVR). However, for many processing operations for cheese, like shredding, dicing, slicing, grating, and mastication, the deformation amplitude and its rate of application are multi-fold higher than the LVR and cross the γ_c of the SAOS region. As a result, linear viscoelastic characterization alone is insufficient to fully understand processing scenarios involving high deformation scales and rates, as SAOS analysis does not disrupt the 3D matrix of the cheese (Yildirim-Mavis, et al., 2022). Thus, for deformations beyond the LVR, nonlinear viscoelastic test protocols, i.e., large-amplitude oscillatory shear (LAOS), can provide useful insights on rheological phenomena (Ewoldt, Hosoi, & McKinley, 2008), such as shear-thinning or shear-thickening and strain-stiffening or strain-softening behaviour of Gouda type cheeses, and how these are affected by freezing treatments. Such rheological information can allow food manufacturers to optimise processing parameters while handling frozen-thawed cheeses.

Yildirim-Mavis, et al. (2022) used LAOS to study the rheological properties of Kashar cheese at high temperature and strain values and observed that the protein network resists progressive deformation of the cheese matrix, resulting in strain-stiffening and pseudoplastic behaviours. Recently, LAOS was used to study the structure development in Mozzarella cheese at different stages of its processing, highlighting the anisotropic dependence of strain stiffening behaviour of pasta filata type cheeses (Dahl, Gregersen, Andersen, Schulz, & Corredig, 2024). Piñeiro-Lago, et al. (2023) used LAOS to study the stress behaviour of acid-curd Spanish cheese (Afuega'l Pitu cheese, pH <4.6) and reported a pseudo-linearity in LAOS response of

121 cheese based on the dominance of rotation (stress-softening) over distortion observed in the
122 normalised elliptical stress-strain plots. Correlation between the viscoelastic, sensory, and oral
123 processing characteristics of Mozzarella, Cheddar, and processed cheeses have also been
124 studied at large deformations, stressing upon the practicality of LAOS techniques (Melito,
125 Daubert, & Foegeding, 2013). These reports indicate a positive trend in the utilization of this
126 comprehensive rheological technique for understanding the viscoelasticity and structure-
127 functionality of cheeses as affected by different processing conditions. However,
128 unfortunately, no reports have detailed the impact of freezing Gouda cheeses at deformation
129 scales relevant to real world usage conditions. Although, one reported study on the application
130 of LAOS to Gouda-type cheese was found (Faber, Van Breemen, & McKinley, 2017). The
131 study reported novel rheological explanations for firmness, rubberiness, and fluidization
132 properties, as well as a new approach to measuring load-induced solid-liquid transitions in very
133 young (3–14 days ripened) Gouda cheese with different fat levels. This, however, excludes
134 mapping the large amount of viscoelastic transitions exhibited by aged Gouda cheese or the
135 impact of freezing treatments.

136 Thus, the present study was designed to understand the impact of two different freezing
137 schemes: (a) prolonged frozen storage (FrS) and (b) multiple freeze-thaw cycles (FTC)
138 application on the thermo-rheological and microstructural properties of aged Gouda cheese
139 using SAOS and LAOS techniques. The FTC application was done to simulate exaggerated
140 temperature fluctuation conditions which could lead to the understanding of adverse effects on
141 the semi-hard cheese matrix due to the loss of controlled frozen conditions or temperature
142 fluctuations during commercial frozen storage and long-distance frozen shipping and retail
143 distribution.

144

2. Materials and Methods

2.1 Cheese sampling and experimental design

Three different batches (vacuum-packed rectangular blocks ~ 15 kg/block/batch; total 45 kg) of industrial Gouda cheese samples manufactured on three different days of the same month were obtained from FrieslandCampina (Amersfoort, The Netherlands). Samples were ripened for a total of 9 months at 6°C in a temperature-controlled room. At the end of 9 months of ripening, each cheese block was portioned into 5 smaller blocks of ~ 3 kg, vacuum-packed, and stored at 6°C until subjected to freezing treatments, which completed within a week. Moisture, fat, salt, protein content and pH of ripened cheeses were determined as described by Page, et al. (2024). Samples were subjected to two different freezing schemes (FTC and FrS). From each batch of portioned cheeses, one randomly picked cheese block was used as an unfrozen control (6°C) sample and analysed within 48 hours of portioning; 3 cheese blocks were randomly picked for the multiple freeze-thaw cycles (FTC) study; and the remaining block of cheese was used for the prolonged frozen storage (FrS) study in a conventional chest freezer at -18±1°C for 3 months. All frozen samples were thawed at 6°C for 48 hours before the analysis and compared against the results of unfrozen control samples.

2.2 Application of multiple freeze-thaw cycles (FTC)

A forced convection air blast freezer (Roeder BGBF-15, Quipman Ireland Ltd.) was used to freeze the cheese samples at -18°C. A Testo 176T4 multichannel data logger (Titisee-Neustadt, Germany) with a chrome-aluminium K-type thermocouple (Fisher Scientific, UK) was used to monitor the temperature at the geometric center of a test Cheddar cheese sample of the same dimension and weight as Gouda cheese blocks, to estimate the freezing time needed to reach a core temperature of -18°C. It took 98±3 min for the 3-kg Cheddar block to reach -

18°C from 5°C (Fig. S1). Hence, the Gouda samples were stored in the blast freezer for 100 minutes to attain a core temperature of -18°C. After that, the samples were stored at 6°C for overnight thawing; this was counted as 1 FTC treatment. For FTC treatments, each block was given either 1 (FTC1), 3 (FTC3), or 5 (FTC5) continuous cycles of freezing-thawing treatments (Fig. S2). The application of freeze-thawing cycles were competed in 5 days. On day 1 of the week, FTC5 samples were subjected to FTC treatments in the blast freezer and, at day 3, FTC3 samples were added to the blast freezer, followed by FTC1 at day 5. Hence, all the FTC treatments were completed by day 5. Samples were analyzed after 48 hours of thawing at 6°C and all the tests were completed within the same week of thawing.

2.3 Small amplitude oscillatory shear (SAOS) rheology

SAOS analysis was performed using an ARG2 rheometer (TA Instruments, New Castle, USA) using a 20-mm serrated steel plate and base Peltier assembly. Cheese samples of 2.0 mm thickness and 20 mm diameter were obtained from the core of the blocks for temperature sweep and frequency sweep analysis. For the temperature sweep test, samples were subjected to 0.5% strain at a frequency 6.28 rad/s, which was within the cheese's LVR region obtained from strain sweep tests. The temperature ramp was performed at a rate of 2°C/min from 7 to 95°C. The outer sides of the samples were glazed with paraffin oil to avoid moisture loss during the tests. The activation energy of flow of the cheese matrix was calculated at two separate temperature ranges, 30-40°C and 70-80°C, to account for the contribution of the fat's liquid or solid state to structural strength. Arrhenius plot (eq. 1, 1a) at 30-40°C and 70-80°C were obtained using complex viscosity ($\eta^* = |G^*|/\omega$) and absolute temperature (T) to calculate the activation energy (E_a; kJ/mol) of cheese melting and deformation.

$$\eta^* = A \times e^{\left(\frac{-E_a}{R.T}\right)} \ldots\ldots\ldots (1)$$

193 $$\ln(\eta^*) = \ln(A) + (-\frac{E_a}{R}) \ln\left(\frac{1}{T}\right) \ldots\ldots (1a)$$

194 Where R (8.314 J $K^{-1}mol^{-1}$) is the universal gas constant, and A is Arrhenius constant.

195 The frequency sweep test was conducted at a constant strain value of 0.5% at 55°C, and the
196 results are interpreted at two different frequency ranges to account for strain application time
197 relevant to practical purposes, i.e., low frequency (LF); 0.06-9.958 rad/s (like spreading), and
198 high frequency (HF) application; 15-99 rad/s (cutting, grating, shredding). The frequency
199 dependence of mechanical moduli were analysed using a power-law model (eq. 2, 3) as
200 suggested by Tunick (2011).

201 $$G' = k_s (\omega)^S \ldots\ldots (2)$$

202 $$G'' = k_L (\omega)^L \ldots\ldots (3)$$

203 Where *S* and *L* are degree of frequency dependency for G' and G", respectively; and k_s and k_L
204 are consistency coefficients.

205

206 **2.4 Large amplitude oscillatory shear (LAOS) rheology**

207 LAOS analysis was performed using a strain-controlled Anton Paar Physica MCR 501
208 rheometer (Anton Paar GmbH, Austria) using the LAOS module in RheoCompass™ software
209 (v1.31). A parallel plate geometry using a sandblasted plate (PP50; diameter 50 mm) and a
210 base Peltier plate were used. Cheese samples of 50 mm diameter and 2 mm thickness, tempered
211 at 6°C for 24 hours (securely wrapped in aluminium foil to prevent moisture loss), were used
212 for the analysis. For every test condition used, i.e., frequency, temperature, strain, and sample
213 type, LAOS produces high-dimensional raw instrumental waveforms of stress-strain data.
214 Hence, for simplifying observations, the test was conducted only at a single frequency of 10
215 rad/s and temperature of 55°C, while using a range of strain values from 0.196 to 360% to

consider large-scale deformations. After sample loading, conditioning for 1 min at 55°C was performed, and the gap was maintained at 2 mm. For plotting Lissajous-Bowditch curves, data visualization, and similarity mapping of the rheological properties, VAOS open source software (source: GitHub at https://vis-au.github.io/vaos/) designed for studying viscoelasticity in soft materials was used (Madsen, Sode, Dahl, Corredig, & Schulz, 2022). A total of 300 points per quarter cycle were used for Fourier transformation and only the 3rd harmonic was considered for comparison of rheological responses (explained in section 2.4.1).

2.4.1 Mathematical background for LAOS analysis

For applied oscillatory strain (> γ_c) or stress > critical stress (σ_c), the output stress or strain waveforms are not sinusoidal due to large deformation amplitudes. However, the raw data can be used to extract useful rheological parameters with physical relevance to changes occurring in the cheese matrix. For the non-sinusoidal stress responses, the dynamic mechanical moduli can be expressed as a function of applied γ and ω, i.e., $G'(\gamma, \omega)$ and $G''(\gamma, \omega)$. The time series of raw instrumental strain and stress data is Fourier-transformed (FT) into frequency domain using infinite sum of sine and cosine functions at progressive harmonics (increasing ω), which constitutes the elastic (eq. 4) and viscous (eq. 5) signatures of the material (Ewoldt, Clasen, Hosoi, & McKinley, 2007).

$$\sigma = \gamma_0 \sum_{n\ odd} \left[G_n'(\omega, \gamma_o) \sin n\omega t + G_n^{"}(\omega, \gamma_o) \cos n\omega t \right] \ldots\ldots\ldots (4)$$

$$\sigma = \dot{\gamma}_0 \sum_{n\ odd} \left[\eta_n^{"}(\omega, \gamma_0) \sin n\omega t + \eta_n'(\omega, \gamma_0) \cos n\omega t \right] \ldots\ldots\ldots (5)$$

where G_n' and $G_n^{"}$ are Fourier coefficients (FC) representing elastic and viscous moduli of nth harmonic; $\eta_n^{"}$ and η_n' are FC representing dynamic viscosities of the nth harmonic; t is time (s); and n represents odd harmonics (1, 3, 5…) in the FT stress waveform and constitutes

useful rheological information. However, higher (>3) and even harmonics are assumed to represent more instrumental noise and testing artefacts e.g., wall slip, secondary flows (Läuger & Stettin, 2010), and thus have not been considered for viscoelastic measurements in this study. The generic nonlinear stress waveforms (eq. 4, 5) were subjected to orthogonal stress decomposition to obtain elastic (σ', Pa) and viscous ($\sigma", Pa$) components (eq. 6, 7)

$$\sigma' = \gamma_0 \sum_{n\ odd} G_n'(\omega, \gamma_0) \sin n\omega t \ \ldots\ldots\ldots (6)$$

$$\sigma" = \dot{\gamma_0} \sum_{n\ odd} G_n"(\omega, \gamma_0) \cos n\omega t \ \ldots\ldots\ldots (7)$$

These viscoelastic moduli are dependent on harmonics used in FT series and the number of harmonics generated are dependent on the applied strain and material properties. Cho, Hyun, Ahn, and Lee (2005) and Ewoldt, et al. (2008) addressed the strain-dependence of material viscoelasticity in the nonlinear region by using Chebyshev polynomials

$$\sigma' = \gamma_0 \sum_{n\ odd} e_n(\omega, \gamma_0) T_n\left(\frac{\gamma}{\gamma_0}\right) \ \ldots\ldots\ldots (8)$$

$$\sigma" = \dot{\gamma_0} \sum_{n\ odd} v_n(\omega, \gamma_0) T_n\left(\frac{\dot{\gamma}}{\dot{\gamma_0}}\right) \ldots\ldots\ldots (9)$$

where, for the n^{th} order harmonic, $e_n(\omega, \gamma_0)$ and $v_n(\omega, \gamma_0)$ are elastic and viscous Chebyshev coefficients, respectively at a given ω and γ_0; and T_n is Chebyshev polynomial of n^{th} order. The relationship between Chebyshev and Fourier coefficients (G_n' and $G_n"$) was established (eq. 10) by Ewoldt, et al. (2008) as:

$$e_n = G_n'(-1)^{\frac{(n-1)}{2}} \text{ and } v_n = \eta_n' = \frac{G_n"}{\omega} \ \ldots\ldots\ldots (10)$$

In this study, only the 3rd order elastic and viscous Chebyshev coefficients were considered for viscoelastic fingerprinting during the SAOS to LAOS transition. Non-linear rheological signatures like intracycle minimum strain (G_M') and large strain (G_L') moduli were obtained from the elastic Chebyshev coefficient e_n by calculating first degree derivative at $\gamma =$

0 and $\gamma = \gamma_0$ based on a deconvoluted stress-strain equation; similarly, intracycle instantaneous viscosity at minimum strain-rate ($\eta'_M;\ \dot{\gamma} = 0$) and large strain-rate ($\eta'_L;\ \dot{\gamma} = \dot{\gamma}_0$) were calculated based on the first degree derivative of the stress-strain rate equation. The parameters G'_L and G'_M refer to intracycle values of elastic modulus at the highest and lowest values of intracycle oscillatory strain application on a sample; this indicates the non-linearity expressed by a samples in terms of ratio (eq. 11) like strain-stiffening (S>0) or strain-softening (S<0). Similarly, η'_L and η'_M correspond to changes in the viscosity of a sample during intracycle strain application and explains shear-thickening (T>0) or shear-thinning (T <0) behaviour (eq. 12) of a sample (Ewoldt, et al., 2008; Seighalani & Joyner, 2019):

$$S(\omega, \gamma_0) = (G'_L - G'_M)/G'_L \ldots\ldots\ldots (11)$$

$$T(\omega, \dot{\gamma}_0) = (\eta'_L - \eta'_M)/\eta'_L \ldots\ldots\ldots (12)$$

Visualization of nonlinear responses was done by plotting normalized intracycle stress (σ) vs. strain (γ), and stress (σ) vs. strain rate ($\dot{\gamma}$) data as elastic and viscous Lissajous-Bowditch (LB) curves, respectively. On an elastic LB plot, at a fixed frequency and temperature, a perfect straight line indicates purely elastic material response whereas a perfect circle indicates purely viscous response. On a viscous LB plot, a purely viscous material is a perfect straight line where as purely elastic response is indicated by a perfect circle. However, a viscoelastic material response is indicated by elliptical shapes with short or long minor axis depending upon whether the material is viscoelastic solid or liquid on an elastic LB plot, respectively (Ewoldt, 2013).

2.5 Visualization of cheese microstructure using confocal laser scanning microscopy (CLSM)

The microstructure of cheese was visualised using a Leica TCS SP5 confocal laser scanning microscope (Leica Microsystems CMS GmbH) as described by Lamichhane, Sharma, Kennedy, Kelly, and Sheehan (2019), with slight modifications. Imaging was conducted with a 20×/0.70 oil immersion objective and a pinhole diameter set to 60.47 au. A digital zoom of 2× was used for all the imaging. Fast Green FCF was excited at 633 nm with a He/Ne laser, and its emission filter was set at 650 to 705 nm. Nile Red was excited at 488 nm with a diode-pumped solid-state laser, and its emission filter was set at 563 to 610 nm. Digital images, 1,024 × 1,024 pixels in size, were acquired using Leica LAS AV software (Leica Microsystems CMS GmbH), with each line averaged four times to improve the signal-to-noise ratio. Each sample was prepared in triplicate, and at least four different areas of each replica were imaged to ensure that images were representative. ImageJ image analysis software package (ImageJ, National Institutes of Health, USA) was used for processing of the micrograph in 8-bit image and for segmentation using color thresholding.

2.6 Statistical analysis

SPSS (Version 27) was used to determine significant differences between the results of rheological analysis at 5% level of significance using one-way analysis of variance (ANOVA) and Tukey's multiple comparison tests was used for paired comparison of treatment means at a 5% level of significance. Two-way ANOVA was used to compare the frequency-dependency of mechanical moduli at high and low frequencies among different FTC and FrS treatments, along with their interactive effects. For each trial, all the analysis were performed at least in triplicate.

3 Results and discussion

3.1 Cheese composition

Gouda cheese samples at the end of ripening and before any freezing treatments (control samples) had on average 41.4±0.6% moisture, 22.5±0.3% protein, 29.2±0.2% fat, 1.6±0.08% salt, and a pH of 5.45±0.02. Freeze-thawing cycles (FTC) and frozen storage (FrS) did not significantly affect cheese composition (Table S1). Similar observations have also been reported for frozen storage studies conducted on other cheese types (Alvarenga, et al., 2011; Van Hekken, Tunick, & Park, 2005).

3.2 Impact of freezing on cheese microstructure

CLSM micrographs (Fig. 1) were subjected to 8-bit image transformation and color thresholding to highlight the microscale gaps created during FTC and FrS treatments. The control sample had a typical cheese microstructure with an interspersed and embedded fat phase in a protein matrix with overall smooth microstructure. The color thresholding indicated minimum empty space (indicated as white patches) as compared to FTC and FrS, which could be micro air pockets left even after cheese pressing during manufacturing. As FTC progressed, changes in micro-gaps can be observed as increased area of white patches. The 8-bit images also indicated more roughening of microstructure with incremental FTC; this could be due to discontinuities created by movement of the water phase during repeated freeze-thawing.

From a microstructural perspective, even a single freeze-thaw cycle had an observable impact. For FTC3, FTC5 and FrS samples, the micro-gaps were comparable, although micro cracks more broader and less in number were prevalent in FTC5 and FrS treatments. This suggests that more water phase pooling and ice recrystallization occurs during repeated freeze-thawing treatments. The FrS treatment created a coarser microstructure with broad empty channels, and similar to this observation, Alinovi, Corredig, Mucchetti, and Carini (2020)

reported the formation of large serum channels in frozen stored (-18°C, 1-4 months) high-moisture Mozzarella, where dehydration of casein and structural expansion due to ice crystal formation were the underlined cause. Also, the minute variation in the microstructure of FrS could be related to the longer exposure of the casein network to cryo-concentrated solute phase leading to changes as discussed in Section 3.5.1. These differences in microstructure relates well to the differences in the diminished thermo-rheological responses obtained through SAOS and LAOS analysis.

Freezing-induced microstructural cracks of varying magnitudes have been reported for Cheddar (Reid, et al., 2004), LMPS Mozzarella (Meng-I Kuo, et al., 2009; Pax, et al., 2023) and ewe's milk cheese (Fontecha, Kaláb, Medina, Peláez, & Juárez, 1996) but no reported study on the microstructure of frozen Gouda cheese or other Dutch cheeses could be found. A longer duration of frozen storage (-20°C, 60 days) was reported to cause a honeycomb-like microstructure with microscale cracks in Mozzarella cheese, which were not observed in very short term frozen-stored (-15°C, 180 min) Mozzarella (Ribero, Rubiolo, & Zorrilla, 2009). However, the pasta-filata process used in the manufacturing of Mozzarella cheese restricts the microstructural comparison with Gouda cheese matrix used in the current study. The scale of differences in micro cracks observed in the reported studies could be due to the differences in cheese type and imaging techniques used like scanning electron microscopy (SEM), cryo-SEM, and transmission electron microscopy (TEM), which may induce artefacts due to sample preparation steps, unlike CLSM.

3.3 Viscoelastic properties measured using SAOS rheology

3.3.1 Impact of freezing on the mechanical moduli (G' and G") of cheese during temperature and frequency sweep tests

359 Viscoelastic responses of the aged Gouda cheese samples within the LVR range were
360 evaluated by temperature and frequency sweep tests. Unfrozen control Gouda samples had
361 higher average G' and G" values (kPa) throughout the temperature range of 7-90°C with
362 notable differences observed at lower temperatures (< 50°C) as compared to FTC and FrS
363 samples (Fig. 2a, 2b). Softening of the cheese matrix upon heating is an obvious thermo-
364 physical change, primarily due to melting of fat, disruption of intra- and inter-protein cross
365 linkages, and heat-induced mobility of moisture and fat in the matrix (Lamichhane, Kelly, &
366 Sheehan, 2018). However, the lower average G' and G" moduli in FTC and FrS samples
367 indicate freezing-induced changes in the structural strength of the cheese matrix. Also, it was
368 observed that FTC treatments, which mimic large-scale temperature shock expected during
369 temperature abuse in long distance shipping and retail distribution, impacted the cheese matrix
370 differently than prolonged and quiescent frozen storage. The FrS treatment caused more loss
371 of elastic characteristics of Gouda cheese than the FTC treatments, which countered the
372 assumption that FTC would result in large-scale macroscopic structural changes in the cheese
373 matrix.

374 The G' and G" values were statistically analysed at 10, 30, and 50°C (Table 1) and both
375 moduli were significantly lower ($P<0.05$) for FrS samples compared to FTC and control
376 samples. For G' values, no statistical difference was found within FTC samples except at 30°C.
377 For G" values, minor differences within FTC samples were observed at 50°C, but these did not
378 significantly differ from the FrS treatment. Overall, a decreasing trend for G' and G" moduli
379 were observed for any freezing treatment applied. A progressive number of freeze thaw cycles
380 did not change the rheological attributes and the rheological impact created in the first FTC
381 remained mostly constant during further FTC application. One possible explanation for this
382 could be the higher rate of cooling achieved using a blast freezer during the rapid FTC
383 treatments i.e., 0.24°C/min as compared to the much slower cooling rate (0.035°C/min) to

384 which FrS samples were subjected while freezing to -18°C prior to frozen storage (Fig. S1).
385 Fontecha, et al. (1996) reported similar findings upon freezing a semi-hard cheese matrix from
386 ovine milk where slow freezing and prolonged frozen storage (-18°C; 4 months) resulted in a
387 pronounced decline in the shear strength and firmness of the cheese structure. Reid, et al. (2004)
388 studied freezing of Cheddar cheese (36-39% moisture) using different fast freezing methods
389 and reported a significant decline in shear strength of all the frozen samples, irrespective of
390 freezing rates used. However, the greater decline in mechanical moduli for FrS samples as
391 compared to FTC could be attributed to the fact that longer duration of frozen storage might
392 provide sufficient time for achieving a moisture-mineral redistribution equilibrium between the
393 regions of concentrated unfrozen serum phase and the casein matrix. Fennema (1972) also
394 highlighted the fact that a longer duration of frozen storage, instead of the freezing process
395 alone, can induce destabilization of proteins.

396 Also, freezing and frozen storage induced changes occurring in the hydration status of the
397 intact and proteolysed fractions of the caseins might also impact the mechanical response of
398 the cheese matrix (McMahon & Oberg, 2017). The hydration behaviour of intact casein
399 micelles indicated that unit mass of casein can associate with ~3.3 g of water, of which ~15%
400 is non-freezable water (primary hydration water or bound water), ~25-30% of water is
401 associated with κ-casein and ~55-60% is physically entrapped by the porous casein micelle
402 (Huppertz, et al., 2017). In aged Gouda cheese, however, extended ripening could lead to a
403 mixture of intact and proteolysed caseins as ~70-80% of α_{s1}-casein and ~50-60% of β-casein
404 is hydrolysed at the end of 6 month of ripening (Berg & Koning, 1990); thus, presenting a blend
405 of water holding capacities of proteins and peptides, with a possible shift in the entrapped
406 fraction of moisture. Buaynov and Buaynova (2016) reported the hydration status of proteins
407 in semi-hard variety of cheeses (~ 44% moisture, ~25% protein) and, based on gross
408 composition, it was observed that ~1.8 g of water was available per gram of cheese protein, of

409 which ~ 0.48-0.54 g g^{-1} protein was termed as bound water or the water fraction constituting
410 mono- and multi-layer hydration associated with the proteolysed caseins, when measured at 0
411 to -10ºC. This is in agreement with the hydration results for intact casein micelles by Huppertz,
412 et al. (2017). However, at -20ºC, the bound water fraction slightly reduced to ~0.39 g g^{-1} of
413 protein, which was attributed to a further crystallization of some multilayer water (binding
414 energy <21.80 kJ/kg moisture) attached at a relatively distant layer from the mono-layer water
415 in cheese proteins (Buaynov, et al., 2016). However, this counters the established notion of
416 bound water as unfreezable water (Tomaszewska-Gras, et al., 2019), but such differences in
417 the hydration behaviour of intact and proteolyticaly broken down caseins could be due to
418 inherent differences in their structural organisation.

419 Upon freezing cheeses, the solubilized minerals (Ca and P), non-protein and amino acids
420 nitrogen, organic acids, and ions (Na^+ and Cl^-) are freeze-concentrated in the serum phase,
421 leading to reduced pH, increased ionic strength and osmotic pressure around the hydrolysed
422 caseins (Reid, et al., 2004). Such changes could result in the dehydration of proteins (Alinovi
423 & Mucchetti, 2020). It has been indicated that partial removal of entrapped moisture from the
424 casein micelle structure can occur upon increased osmotic stress or ultracentrifugation for
425 longer periods (Huppertz, et al., 2017). Such moisture redistribution could happen more during
426 the FrS (longer moisture equilibration time i.e., 90 days at -18°C) treatment than rapid FTC
427 treatments; thus, a more dehydrated protein network could lead to lower G' and G" values in
428 FrS samples as compared to FTC and control samples. M-I Kuo and Gunasekaran (2003) and
429 Guinee and Fox (2017) also reported the possibility of a partially dehydrated and weaker casein
430 matrix in freeze-thawed cheeses. Similar findings on the behaviour of casein micelles under
431 high osmotic stresses have also been reported by Famelart, Le Graet, and Raulot (1999).

432 The rapid FTC treatments seems to freeze-thaw and refreeze only the serum moisture
433 (freezable moisture) and apparently little to no movement of multi-layered water occurs in this

short duration, hence, the hydration status of proteolysed caseins is not changed to the same extent as in the case of FrS treatment. The decline in the G' and G" values in the FTC samples could exclusively be a result of physical expansion of the matrix due to water and fat crystallization, as observed from the CLSM micrographs (Fig. 1) . Van Hekken, et al. (2005) reported a reduction in viscoelastic properties upon very short term frozen storage (2 days, -20 ^{o}C) of soft caprine milk cheeses, hence, the impact of FTC treatments seems to remain more or less similar to other cheese matrixes as well; but, there is a gap in such published reports.

3.3.2 Activation energy (E_a) of flow and frequency dependence of mechanical moduli in the SAOS region

Microstructural changes and flow of the cheese matrix upon heating are an important functional and rheological attribute. The changes in δ (in rad; ratio of G"/G') during temperature sweep analysis indicates relaxation of intra- and inter protein-protein, protein-peptide and peptide-peptide bonds, and the maximum value of δ (δ_{max} at temperature $T_{\delta\text{-}max}$; °C) is also used to infer the melt or flow behaviour of cheeses (Sharma, Munro, Dessev, & Wiles, 2016). In the present study, however, no significant differences in δ_{max} and $T_{\delta\text{-}max}$ values were observed (Table 2) for any freezing treatments. As an alternative approach, Joyner (2019) reported that the thermo-rheological flow of materials can be comprehensively explained using structural rigidity (G*; complex modulus) or deformability (η*; complex viscosity) indices. Thus, the activation energy (E_a, kJ/mol) of the cheese matrix, i.e., the energy required for its deformation and flow, was calculated, as it can account for the indices like G* or η* (see eq. 1, 1a).

The contribution of fat to network strength is highly temperature dependent and the mechanical response of the cheese matrix rapidly declined (Fig. 2c) after the onset, until the

completion of fat melting in the range 30-40°C, and also due to limited softening of protein network. Freezing impacts the polymorphic and crystallization status of fats and modifies the physical protein-fat interaction behaviour (Alinovi & Mucchetti, 2020; Buldo, Andersen, & Wiking, 2013). A typical range for latent heat of fusion of bovine milk fat ranges between 70-80 J/g of fat (Tunick, 2010). Thus, to account for such factors, E_a before (E_a-t; 30-40°C) and after (E_a-T; 70-80°C) the complete liquefaction of fat was calculated. The E_a-t values for control, FTC and FrS cheese samples were in the range 100-110 kJ/mol and did not significantly differ (Table 2, Fig. S3). Similar E_a values (100-150 kJ/mol at 30-45°C) were reported for Cheddar and Mozzarella type cheeses by Tunick (2010). At higher temperatures (70-80°C), the overall average E_a-T significantly ($p < 0.05$) decreased to ~27-48 kJ/mol for all the samples, which is expected due to the complete loss of structure-forming ability of the fat component (Lamichhane, et al., 2018). However, in this temperature range, the E_a for FTC or FrS samples were higher than for the control samples. This effect could be due to the partial dehydration of the protein network (discussed in previous section), which might present higher resistance to initiate an actual flow due to the loss of lubrication (from fat, moisture), and polymorphic transitions like sintering of fat crystals could have altered the environment around the protein phase (Buldo, et al., 2013).

Udyarajan, Horne, and Lucey (2007) reported the possibility of heat-induced associations at high temperatures (80-90°C) within a residual protein network by binding of some calcium and phosphate ions as insoluble calcium precipitates, as observed from the increased elastic properties of Cheddar cheese at 80-90°C. Also, it appears that, in the low temperature (30-40°C) region, a pronounced effect of fat melting on mechanical moduli could mask the actual impact of freezing treatments on the protein bonds. This is evident from no significant change (Table 2) in the crossover temperature (53.2±1.6°C) for any freezing treatments, which strongly

indicates that the fat phase could actually provide a cushioning effect during network compression and expansion. Similar observations on thermo-rheological response during melting of fat free cheeses were reported by Lucey, Johnson, and Horne (2003), where relaxation of protein bonds in cheese started at temperatures >40°C. Thus, it appears that measuring E_a of freeze-thawed cheeses at temperatures above the complete liquefaction of fat could be more useful in measuring the impact of freezing on the protein matrix. Tunick (2010) reported E_a (at 30-45°C) values of 30-60 kJ/mol for non-melting caprine cheese and Queso Fresco cheeses, and E_a >180 kJ/mol for rapidly flowable Parmesan (very hard) cheese. This indicates that the high E_a only depicts an initial higher resistance in initiating the flow and deformation; however, it does not indicate the extent of melting a cheese matrix can achieve when supplied with energy >>E_a.

A frequency sweep analysis was done at 55°C (closer to the crossover temperature) in order to avoid structural contribution from the solid fat, ensuring sufficiently softened protein phase and yet avoiding major heat-induced changes in the cheese matrix. This temperature is also close to the practical consumption temperatures of cheeses. Power-law fitting was performed at low frequency (LF: 0.06-9.958 rad/s) and at high frequency (HF: 15-99 rad/s) to understand the frequency dependency of G' and G" (Fig. 2d, Table S2). The G' value was found to be more sensitive to frequency changes than G" for all the treatments. Frequency dependence (or Power-law factor) of storage modulus at low frequency (*S*-LF: 0.584 – 0.784) was higher than at high frequency (*S*-HF: 0.460 – 0.488) and the *S*-LF declined from 0.723±0.074 to 0.584±0.062 with incremental FTC treatments, while FrS and control samples had no significant differences (Table S2). Similar findings of high frequency dependence of G' modulus for refrigerated and frozen low-fat soft cheese has been reported by Meza, et al. (2011). Also, no change was reported in the frequency dependence (0.633 – 0.668) of the G'

values of control and quiescent frozen stored (-20°C, 1-3 months) LMPS Mozzarella cheese, tested at 60°C (Diefes, Rizvi, & Bartsch, 1993).

For both G' and G" values, no significant differences in frequency-dependence were observed at HF for any applied freezing treatments; while frequency-dependency for both G' and G" significantly ($p< 0.05$) reduced with progressive freeze-thaw treatments at LF. Thus, at a low frequency of strain application, calculation of frequency-dependency of either G' or G" could serve as a useful indicator to evaluate whether or not the frozen stored cheese matrix had been exposed to rapid and large scale temperature abuse.

3.4 Measurement of viscoelastic properties using LAOS rheology

3.4.1 Intracycle moduli, shear thinning and strain stiffening behaviour of cheese as affected by freezing treatments

The plot for intracycle large (G'_L) and minimum (G'_M) strain moduli versus strain (0.196-360%) indicated a strong strain-dependent decline for all the treatments (Fig. 3a, 3c). In comparison with the control samples, FTC samples had a lower average values for both the moduli throughout the strain range. Also, the rate of loss of G'_L and G'_M for FTC samples were maximum during transitioning at lower γ values (0.1-1%), which indicates initiation of the breakdown of intact protein network in cheese. However, the FrS samples showed a lower rate of decline in G'_L and G'_M in this region as compared to FTC samples and a continued plateauing (minimum rate of intracycle decline) of moduli was observed in the region $0.1< \gamma <10\%$. This indicates a lower residual intact casein matrix structure in FrS samples in the SAOS region as compared with control and FTC samples. The strain sweep test during LAOS analysis (Fig. 3f; Fig. S4) also confirmed the lowest G' and G" values for FrS samples near transitioning of the SAOS region, complimenting the observations under SAOS (Fig. 2a, 2b) test conditions that

the duration of frozen storage causes more loss in the G' and G" values to the cheese matrix than rapid temperature fluctuations.

The plateauing of G'_L and G'_M values (Fig. 3a, 3c) were also observed in FTC samples in the strain range 1-10%. Plateauing of the moduli could be due to the dynamics of simultaneous bond breaking and bond formations (due to emergence of new binding sites, and thus new hydrogen bonding and hydrophobic interactions) in the proteolysed caseins (as the temperature of analysis remained at 55°C). Also, as the applied strain range is relatively moderate (<10%), large scale irreversible disruption in matrix might not have occurred. Such intermediate changes, especially the formation of transient inter protein linkages upon supply of thermal energy have been reported in cheese matrices (Sharma, et al., 2016) as they are categorised as weak physical gels (Lucey, et al., 2003). At γ >1%, the intracycle moduli for FrS samples (Fig. 3a, 3c) exhibited near complete congruence with the control samples, which could be due to the formation of new bonds within and between aggregated proteins, involving a limited re-association of calcium from the soluble phase (see section 3.3.2).

For all the treatments, plateauing of G'_L and G'_M ended at ~ $\gamma > 10$ and a rapid decline was observed afterwards (Fig. 3a, 3c). This phenomenon is a typical representation of strain transitioning from medium to large strain region, which could abruptly break the residual protein-protein bonds and transient structural gains that may have occurred during the plateauing region. Yildirim-Mavis, Yilmaz, Dertli, Arici, and Ozmen (2019) studied sourdough, where gluten was the principal structure-forming protein, using LAOS; a similar transitioning of intracycle moduli was observed between SAOS to LAOS regions and a region of moderate strain values was referred to as the medium amplitude oscillatory shear (MAOS) region i.e., ~γ=5.2%. However, due to inherent differences between casein and gluten, and the absence of colloidal or soluble calcium in the latter, any plateauing was not observed in the MAOS region. In the present study, the strain range 1< γ <10 % could be considered as the

MAOS region (also the plateauing region) where the rate of decline in the intracycle moduli remains minimal.

The transient network rearrangements during structural collapse could lead to either shear-dependent (Fig. 3b) thickening (T>0) or thinning (T<0) or strain-dependent (Fig. 3d, 3e) structural stiffening (S>0) or softening (S<0). The mathematical background for the above has been given in eq. 11, 12. Intracycle viscosity at large strain-rate (η'_L) and minimum strain-rate (η'_M) also followed a similar declining trend (Fig. S5) as G'_L and G'_M for the range of applied strain; however, the magnitude of intracycle differences between η'_L and η'_M were low as compared to the differences in G'_L and G'_M. This reflected a more strain-stiffening behaviour (Fig. 3d, 3e) at large deformations (γ>10%), as well as transient shear-thickening at γ ~100% (FTC and control samples) and shear-thinning beyond ~ γ >100% (in all samples, Fig.3b). Similar results were reported for cream cheese, where a prominent strain-stiffening and significant shear-thinning were observed at γ>10% (Q. Wang, Espert, Hernández, Salvador, & Sanz, 2024), indicating the complex non-linear rheological transitions exhibited by cheeses at higher deformations. The difference between G'_L and G'_M or η'_L and η'_M remained ~ 0 until the end of the MAOS region (Fig. 3b, 3d), which suggests that, at low to moderate strain values, disruptive intracycle changes in protein-protein interaction does not occur, irrespective of freezing treatments applied.

However, beyond the MAOS region (γ >10%), prominent strain-stiffening (S>0) and comparatively less intense shear-thinning (T<0) behaviour was observed for all the treatments. The rate of stiffening was higher at γ >100 % than at 10< γ <100 % (Fig. 3d, 3e). Higher oscillatory strain amplitude might induce a directional pattern of displacement and physical alignments in the aggregated, softened casein-fat matrix (temperature of analysis 55°C), which could promote faster expulsion of melted fat from the matrix, thereby minimizing the lubrication in the rearranged protein network. Shear-thinning (T<0) behaviour (Fig. 3b), i.e., a

reduction in intracycle dynamic viscosity at γ >100% also compliments this observation. Similar findings were also reported at high strain and temperatures for Kasher cheese, a semi-hard cheese variety (Yildirim-Mavis, et al., 2022).

The FrS samples exhibited lowest strain-stiffening and highest shear-thinning behaviour (Fig. 3b, 3d, 3e) as compared to FTC or control samples (at γ >100%). This could be due to less expulsion of liquid fat from the matrix, possibly due to an increase in residual crystalline fat content as a result of polymorphic changes in fats during prolonged frozen storage (Buldo, et al., 2013). Minor shear-thickening (Fig. 3b) in control and FTC samples at γ ~100 % followed by rapid shear-thinning in all the treatments at γ >100% indicates a sequential interplay of partial protein-hydration, followed by rapid fat expulsion from the matrix at higher strains, as discussed before.

3.4.2 Evaluation of normalised non-linear rheological responses using elastic and viscous Lissajous-Bowditch plots

The aged Gouda cheese (FrS, FTC, and control) in this study were subjected to 26 shear strain values in increasing order from 0.196 to 360% and the stress responses were recorded to calculate different non-linear rheological parameters. Normalized intracycle stress responses (σ/σ_o) were plotted against normalised strain (γ/γ_o) and strain-rate ($\dot{\gamma}/\dot{\gamma}_o$) to obtain elastic and viscous Lissajous-Bowditch (LB) plots, respectively. Elastic and viscous LB plots at different strain values on x-axis and freezing treatments on y-axis were plotted as Pipkin diagrams (Fig. 4). To account for the visual transition of viscoelastic response from SAOS, MAOS and LAOS regions, 5 pertinent strain values i.e., 0.196, 1.19, 59.3, 197, and 360% were selected, representing every region.

For all the treatments, at strain values of 0.196 and 1.19% on an elastic LB plot (Fig. 4a), an elliptical shape with short minor axis indicates the viscoelastic solid characteristics of the matrix, a typical response in close proximity to the SAOS region, although the applied frequency (10 rad/s) was higher than used for SAOS. Within the treatments at low strain values (0.196-1.19%), minor increase in the area (Fig. 4a) of ellipse for FrS and FTC samples (FrS> FTC) are indicative of energy dissipated by the matrix at these strain values, which confirms a greater loss of elastic characteristics in FrS samples than FTC samples. However, as γ progresses >1.19%, the viscoelastic response undertakes an elliptical shape with increasing minor axis and, at γ >59.3%, a rectilinear shape appeared with increasing area under the curve, indicative of a transition to dominant viscoelastic-liquid characteristics (Ewoldt, 2013). A concomitant change in the profile of viscous LB plots can be observed (Fig. 4b) where the broader elliptical shapes at low strain values indicates more solid-like characteristics (0.196< γ<1.19%) and, as strain progresses (> 59.3%), narrow ellipses with short minor axis are linked to a viscoelastic-liquid response of the material. The area under the ellipse on viscous LB plots is indicative of energy stored by the material (Joyner, 2019) and a decline in the area at γ >59.3% compliments the finding of an elastic LB response.

Distortion and rotation of the rectilinear shapes on elastic LB plots started to appear at $\gamma > 100\%$ (plots only shown for 197% and 360%). While the distortion was dominant at high strain values ($\gamma = 197\%$), rotation of curve was dominant at extremely high strains ($\gamma = 360\%$). At very large strains, the disruption of residual protein-protein bonds is almost complete and macroscopic oscillation of structural alignment at large oscillatory strain and harmonic shifts in some structural elements during increasing cycles of freezing-thawing treatments might lead to the rotation of shapes rather than distortion. Also, the rectilinear shapes for control and FrS samples are qualitatively similar; however, for FTC treatments, more rotational changes were observed at higher strain values (γ >197%) than FrS, which further consolidates the evidence

of structural shifts during freeze-thawing cycles. Ewoldt, et al. (2008) reported that clockwise and counter-clockwise rotation of ellipses on an elastic-LB plot relates to strain-stiffening and softening of material, respectively. From quantitative analysis (eq. 11) and qualitative observation of the rotations, the strain-stiffening ratio was found to increase for all the treatments in this study at $\gamma > 100\%$; however, a trend in the order of control >FTC (1-5) >FrS suggests that rapid freezing-thawing, as well as frozen storage, alters the physical environment within which protein, fat, and moisture interacts. But the lowest value for FrS could be a result of increased polymorphic crystallization of the fat phase during prolonged frozen storage (observed through Raman spectroscopic analysis in wavenumber region 3000-2800 cm^{-1}; data not shown), resulting in lesser fat expulsion from the matrix as compared to FTC and control. Similar rotation, rather than deformation, of shapes on elastic LB plots were reported for Mozzarella cheese at higher strain values (~1000 %) and temperatures (10-80°C) by Dahl, et al. (2024).

The secondary loops in elliptical shapes on viscous LB plots were observed at higher strain-rate (γ >197%) for all the treatments with varying magnitude (secondary loop in FrS sample shown in Fig. 5). Ewoldt and McKinley (2010) presented a mathematical interpretation of this as a repetition of the stress response of the material at a given strain-rate. This supports observations of shear-thinning behaviour at intracycle higher strain values and indicates time-dependent shear-thinning or thixotropic behaviour of aged Gouda cheese. However, the variations within the FTC samples for secondary loops were visibly higher than for FrS and control samples at $\gamma = 360\%$. Such results indicate heterogeneity induced in the matrix due to rapid freeze-thawing treatments, which might create localised zones of varying yield and flow behaviours within the cheese matrix due to repeated thermal stress. Here, any possibility of rheological artefacts due to sample preparation and during the analysis could safely be ruled out due to uniformity in sampling process and the use of cross-hatched parallel plate geometry,

654 which virtually eliminates any wall-slips (Dahl, et al., 2024). The observation of a secondary
655 loop at higher strain values (Fig. 4b) for all the treatments is indicative of strong non-linearity
656 in the elastic behaviour of the samples (Hyun, et al., 2011). Similar secondary loops at higher
657 strain-rate have been observed in materials like polystyrene solutions, tomato paste, and guar-
658 gum based solutions (Joyner, 2019). The presence of secondary loops in stress-strain plots
659 represents strong non-linearity in the viscous behaviour of the material (Ewoldt, et al., 2010).

660

661 **3.4.3 Similarity maps for Lissajous-Bowditch plots**

662 Similarity mapping of elastic and viscous responses obtained on respective LB curves is
663 shown in Figure 6. The VAOS tool enables comparing the relative positions of elastic or
664 viscous responses of samples at various strain values from a perfectly elastic or viscous
665 reference points (Dahl, et al., 2024). The approximate linear distance from the reference points
666 is indicated (Fig.6a, 6b) as D_γ and d_γ at various γ values on elastic and viscous similarity maps,
667 respectively. In the elastic similarity map (Fig. 6a), the stress responses at very low strain
668 (0.196-1.19 %) values indicated closest proximity to perfect elastic reference point and, as the
669 strain value increased (59.3, 197 and 360%), the approximate distance of grouped responses
670 increased as well, which indicated strain-dependent evolution of viscoelastic liquid behaviour.
671 Also, the relative positional distribution within the treatments at low to moderate strain values
672 (γ <59.3%) were very narrow, which indicated that FTC and FrS samples generated similar
673 stress responses in the strain range close to LVR regions, although the exact position with
674 respect to the reference point showed minor variations, and these variation in mechanical
675 responses have been successfully quantified in terms of G' and G" using SAOS analysis.

676 At moderate strain value (59.3%), $D_{59.3}$ increased, which indicates that the loss of elastic
677 properties is more due to increased % strain rather than freezing treatments as, within the

678 treatments, variations were still minimum. However, at higher strain values ($\gamma > 100\%$; only
679 197 and 360 % have been indicated), a broader spread within the treatment groups were
680 observed. This was evident from the differences in the trend for strain-stiffening and shear-
681 thinning values of FrS, FTC and control samples at $\gamma >$100%. Thus, the impact of freezing on
682 semi-hard cheeses could be more prominently observed during practical deformation scenarios
683 like cutting, shredding, grating, stretching, and chewing. Since the LAOS analysis in this study
684 was limited to 55°C, which is close to the obtained cross-over temperature (53.2±1.6°C), the
685 results are indicative of the performance of semi-hard cheese at large strains with completely
686 melted fat inside the matrix. As discussed in previous sections, that un-melted fat phase could
687 actually mask the real impact of freezing on the structural strength of the protein network.

688

689 **3.4.4 Evaluation of rheological non-linearity using un-normalised Lissajous-Bowditch**
690 **plots**

691 Normalisation of stress-strain values provides useful visual qualitative information
692 regarding rheological evolutions in samples; however, it may mask quantitative differences in
693 the deformation behaviour of samples (Dahl, et al., 2024; Yildirim-Mavis, et al., 2019). Hence,
694 un-normalised stress vs. strain and stress vs. strain-rate as 2D-layover strain plots at five
695 different strain values (0.196, 1.19, 59.3, 197, and 360%) for control, FTC5 and FrS samples
696 are presented in Figure 7. Also, a representation of elastic and viscous components of
697 cumulative stress responses at two strain levels (low- 0.196% and high- 360%) is indicated as
698 un-normalised 3D elastic and viscous Lissajous-Bowditch plots (Fig. 8). Both the size and
699 distortion of elliptical shapes (Fig. 7) increased with % strain, but qualitative and quantitative
700 variability at 0.196 and 1.19% strains (see color coding) could not be detected due to the
701 minuscule elliptical projection of elastic and viscous stress responses. This aligns with the

previous observation that freezing has a limited impact on rheological attributes at deformation scale and rates irrelevant to practical applications. Even at moderate strain values ($\gamma \leq 59.3\%$), viscoelasticity dominates irrespective of freezing treatments applied, which is apparent from the enlarging but not distorting elliptical shaped stress-strain response. Such responses are typical of pseudo-linearity shown by cheese matrices (Piñeiro-Lago, et al., 2023), which could be due to the formation of transient structures (see section 3.4.1) during low to moderate controlled strain application.

These temporary protein/peptide bonds are dependent on factors like ripening stage, calcium content distribution, and protein-fat ratio, as well as extrinsic factors like temperature and time scale of rheological measurements (Fox & McSweeney, 1996). However, for $\gamma \geq 59.3\%$, horizontal comparisons within the treatment groups reveal qualitative changes in elastic and viscous responses. Also, the increased distortion of ellipse is concomitant with the loss of elasticity in all the treatments but the distortion in FrS and FTC samples were higher at $\gamma = 360\%$. This is consistent with the observation that freezing has a perceptible impact on the cheese matrix in practical deformation scenarios, as previously discussed.

The stress responses on 3D-stress vs. strain and strain-rate plots indicated minor distortional and rotational variations (Fig. 8) within FTC samples at low strain, i.e., 0.196%. The distortion in the ellipse is perceivable starting from first freeze-thaw cycle when compared with the control samples, and the shape and orientation of ellipse remained almost unchanged for increasing FTC treatments; the lack of significant differences in G' and G" modulus (Table 1) within the FTC treatments (except for the G' of FTC1 sample at 30°C; $p<0.05$) supports this observation. Thus, rapid freeze-thawing leads to microstructural shifts that cause minor rheological differences. Moreover, these microscale differences in FTC samples were not as prominent as the differences quantified for frozen stored samples. At higher strain (360%), distortion in the elliptical stress responses increased for all the samples, in line with the loss in

viscoelasticity. Application of freeze-thawing cycles (1-5 cycles) on caprine milk cheese with low protein (~15%) and high moisture (48%) content was reported to greatly damage the cheese texture (X. Wang, Li, & Zhao, 2023), but the contrasting compositional and ripening differences with the cheese matrix used in the present study does not allow clear comparison of the results. The higher resistance to rapid freeze-thaw cycles in semi-hard matrices could be due to low moisture content which, in turns, results in less expansion during freezing. Also, the high protein content in cheese matrix reduces freezable water content (as more water is bound to caseins) and results in closer packing of the network; thus, increased resistance to structural damage due to ice crystallization could be assumed.

4. Conclusions

Application of small and large amplitude oscillatory shear rheology was found to compliment the broader understanding of freeze-induced structural changes in semi-hard Gouda cheese. SAOS analysis showed that both FTC and FrS type treatments caused loss of structural strength within the protein-fat matrix, but the loss was higher in frozen stored samples. The calculation of activation energy of flow at or above temperatures ensuring complete liquefaction fat could give better information on the effects of freezing on the protein matrix. In the present study, longer frozen storage caused an increase in activation energy of flow at higher temperatures, indicating increased fat crystallization, dehydration and stiffening of the protein matrix. The strain-stiffening (S) and shear-thinning (T) ratios, calculated using intracycle moduli (G_L', G_M', η_L' and η_M') obtained from LAOS analysis, quantified the impact of freeze-thawing or frozen storage of a semi-hard cheese matrix pertinent to practical deformation situations. Microstructural observations also aligned with these findings. Although the application of multiple freeze-thawing in the present study was intended to

exaggerate the situation of temperature fluctuations, in practical scenarios, however, the temperature abuse would not normally match this scale. Hence, from a rheological perspective, it was observed that semi-hard matrices are fairly inert to short and rapid temperature deviations (relevant to practical conditions). Elastic and viscous Lissajous-Bowditch plots and similarity mapping presented a complete rheological fingerprinting of the semi-hard cheese matrix, as affected by freezing treatments. Similar studies on other cheese types of different ripening status and composition could provide broader understanding of freezing-induced changes relevant to practical application conditions.

Acknowledgements

Digvijay is a recipient of a Walsh Scholarship from Teagasc, the Irish Agricultural and Food Development Authority (Ref 2022059). We thank FrieslandCampina Netherlands for providing the Gouda cheese samples.

Declaration of competing interest

The authors declare that they have no known competing financial interests to influence the work reported in this paper.

References

Alinovi, M., Corredig, M., Mucchetti, G., & Carini, E. (2020). Water status and dynamics of high-moisture Mozzarella cheese as affected by frozen and refrigerated storage. *Food Research International, 137*, 109415.

Alinovi, M., & Mucchetti, G. (2020). Effect of freezing and thawing processes on high-moisture Mozzarella cheese rheological and physical properties. *Lwt, 124*, 109137.

776 Alinovi, M., Mucchetti, G., Wiking, L., & Corredig, M. (2021). Freezing as a solution to preserve the
777 quality of dairy products: The case of milk, curds and cheese. *Critical Reviews in Food Science*
778 *and Nutrition, 61*(20), 3340-3360.
779 Alvarenga, N., & Sousa, I. (2011). Effect of freezing on the rheological, chemical and colour properties
780 of Serpa cheese. *Journal of dairy research, 78*(1), 80-87.
781 Berg, G. v. d., & Koning, P. d. (1990). Gouda cheesemaking with purified calf chymosin and microbially
782 produced chymosin.
783 Bertola, N., Califano, A., Bevilacqua, A., & Zaritzky, N. (1996). Effect of freezing conditions on functional
784 properties of low moisture Mozzarella cheese. *Journal of Dairy Science, 79*(2), 185-190.
785 Buaynov, O., & Buaynova, I. (2016). The physical and chemical changes of water and the hydration of
786 the protein complex in cheese during freezing. *Foods and Raw materials, 4*(1), 13-18.
787 Buldo, P., Andersen, U., & Wiking, L. (2013). Microstructure and material properties of milk fat systems
788 during temperature fluctuations. *Food Biophysics, 8*, 262-272.
789 Cho, K. S., Hyun, K., Ahn, K. H., & Lee, S. J. (2005). A geometrical interpretation of large amplitude
790 oscillatory shear response. *Journal of Rheology, 49*(3), 747-758.
791 Dahl, J. F., Gregersen, S. B., Andersen, U., Schulz, H.-J., & Corredig, M. (2024). Small and large
792 deformation rheology on pizza cheese as an example of application to study anisotropic
793 properties of food soft materials. *Food Hydrocolloids, 148*, 109456.
794 Diefes, H. A., Rizvi, S., & Bartsch, J. (1993). Rheological behavior of frozen and thawed low-moisture,
795 part-skim Mozzarella cheese. *Journal of Food Science, 58*(4), 764-769.
796 Digvijay, Kelly, A. L., & Lamichhane, P. (2023). Ice crystallization and structural changes in cheese
797 during freezing and frozen storage: implications for functional properties. *Critical Reviews in*
798 *Food Science and Nutrition*, 1-24.
799 Ewoldt, R. H. (2013). Defining nonlinear rheological material functions for oscillatory shear. *Journal of*
800 *Rheology, 57*(1), 177-195.
801 Ewoldt, R. H., Clasen, C., Hosoi, A. E., & McKinley, G. H. (2007). Rheological fingerprinting of gastropod
802 pedal mucus and synthetic complex fluids for biomimicking adhesive locomotion. *Soft Matter,*
803 *3*(5), 634-643.
804 Ewoldt, R. H., Hosoi, A., & McKinley, G. H. (2008). New measures for characterizing nonlinear
805 viscoelasticity in large amplitude oscillatory shear. *Journal of Rheology, 52*(6), 1427-1458.
806 Ewoldt, R. H., & McKinley, G. H. (2010). On secondary loops in LAOS via self-intersection of Lissajous–
807 Bowditch curves. *Rheologica acta, 49*, 213-219.
808 Faber, T., Van Breemen, L., & McKinley, G. (2017). From firm to fluid–Structure-texture relations of
809 filled gels probed under Large Amplitude Oscillatory Shear. *Journal of Food Engineering, 210*,
810 1-18.
811 Famelart, M.-H., Le Graet, Y., & Raulot, K. (1999). Casein micelle dispersions into water, NaCl and
812 CaCl2: physicochemical characteristics of micelles and rennet coagulation. *International Dairy*
813 *Journal, 9*(3-6), 293-297.
814 Fennema, O. (1972). Freezing of cheese-pros and cons. *Western milk ice cream news, 20*.
815 Fontecha, J., Kaláb, M., Medina, J. A., Peláez, C., & Juárez, M. (1996). Effects of freezing and frozen
816 storage on the microstructure and texture of ewe's milk cheese. *Zeitschrift für Lebensmittel-*
817 *Untersuchung und Forschung, 203*, 245-251.
818 Fox, P., & McSweeney, P. (1996). Proteolysis in cheese during ripening. *Food Reviews International,*
819 *12*(4), 457-509.
820 Gelder, K. v. (2023). Value of the import and export of Gouda cheese in the Netherlands 2008-2021.
821 In (Vol. 2024): Statista.
822 Guinee, T. P., & Fox, P. F. (2017). Salt in cheese: physical, chemical and biological aspects. In *Cheese*
823 (pp. 317-375): Elsevier.
824 Huppertz, T., Gazi, I., Luyten, H., Nieuwenhuijse, H., Alting, A., & Schokker, E. (2017). Hydration of
825 casein micelles and caseinates: Implications for casein micelle structure. *International Dairy*
826 *Journal, 74*, 1-11.

827 Hyun, K., Wilhelm, M., Klein, C. O., Cho, K. S., Nam, J. G., Ahn, K. H., Lee, S. J., Ewoldt, R. H., & McKinley,
828 G. H. (2011). A review of nonlinear oscillatory shear tests: Analysis and application of large
829 amplitude oscillatory shear (LAOS). *Progress in polymer science, 36*(12), 1697-1753.
830 Johnston, D. (2000). The effects of freezing at high pressure on the rheology of Cheddar and
831 Mozzarella cheeses. *Milchwissenschaft, 55*(10), 559-562.
832 Joyner, H. S. (2019). *Rheology of semisolid foods*: Springer.
833 Kasprzak, K., Wendorff, W., & Chen, C. (1994). Freezing qualities of Cheddar-type cheeses containing
834 varied percentages of fat, moisture, and salt. *Journal of Dairy Science, 77*(7), 1771-1782.
835 Kuo, M.-I., & Gunasekaran, S. (2003). Effect of frozen storage on physical properties of pasta filata and
836 nonpasta filata Mozzarella cheeses. *Journal of Dairy Science, 86*(4), 1108-1117.
837 Kuo, M.-I., & Gunasekaran, S. (2009). Effect of freezing and frozen storage on microstructure of
838 Mozzarella and pizza cheeses. *LWT-Food Science and Technology, 42*(1), 9-16.
839 Lamichhane, P., Kelly, A. L., & Sheehan, J. J. (2018). Symposium review: Structure-function
840 relationships in cheese. *Journal of Dairy Science, 101*(3), 2692-2709.
841 Lamichhane, P., Sharma, P., Kennedy, D., Kelly, A. L., & Sheehan, J. J. (2019). Microstructure and
842 fracture properties of semi-hard cheese: Differentiating the effects of primary proteolysis and
843 calcium solubilization. *Food Research International, 125*, 108525.
844 Läuger, J., & Stettin, H. (2010). Differences between stress and strain control in the non-linear behavior
845 of complex fluids. *Rheologica acta, 49*(9), 909-930.
846 Lucey, J., Johnson, M., & Horne, D. (2003). Invited review: Perspectives on the basis of the rheology
847 and texture properties of cheese. *Journal of Dairy Science, 86*(9), 2725-2743.
848 Madsen, J., Sode, L., Dahl, J. F., Corredig, M., & Schulz, H.-J. (2022). Visual Exploration of Rheological
849 Test Results from Soft Materials. In *2022 First International Workshop on Visualization in*
850 *Testing of Hardware, Software, and Manufacturing (TestVis)* (pp. 1-7): IEEE.
851 McMahon, D. J., & Oberg, C. J. (2017). Pasta-filata cheeses. In *Cheese* (pp. 1041-1068): Elsevier.
852 Melito, H., Daubert, C., & Foegeding, E. (2013). Relationships between nonlinear viscoelastic behavior
853 and rheological, sensory and oral processing behavior of commercial cheese. *Journal of*
854 *Texture Studies, 44*(4), 253-288.
855 Meza, B. E., Verdini, R. A., & Rubiolo, A. C. (2011). Effect of freezing on the viscoelastic behaviour
856 during the ripening of a commercial low-fat soft cheese. *International Dairy Journal, 21*(5),
857 346-351.
858 Oberg, C. J., Merrill, R. K., Brown, R. J., & Richardson, G. H. (1992). Effects of freezing, thawing, and
859 shredding on low moisture, part-skim Mozzarella cheese. *Journal of Dairy Science, 75*(5), 1161-
860 1166.
861 OECD/FAO. (2021). *OECD-FAO Agricultural*
862 *Outlook 2021-2030*. Paris: OECD Publishing.
863 Page, R. M., Magan, J. B., Mannion, D. T., Kilcawley, K. N., Murphy, J. P., Kennedy, E., O'Donovan, M.,
864 Tobin, J. T., O'Mahony, J. A., & O'Callaghan, T. F. (2024). The impacts of milking frequency on
865 nutrient composition and functional characteristics of Cheddar cheese. *International Journal*
866 *of Dairy Technology, 77*(3), 630-644.
867 Pax, A. P., Ong, L., Pax, R. A., Vongsvivut, J., Tobin, M. J., Kentish, S. E., & Gras, S. L. (2023). Industrial
868 freezing and tempering for optimal functional properties in thawed Mozzarella cheese. *Food*
869 *Chemistry, 405*, 134933.
870 Piñeiro-Lago, L., Ramlawi, N., Franco, I., Tovar, C. A., Campo-Deaño, L., & Ewoldt, R. H. (2023). Large
871 amplitude oscillatory shear stress (LAOStress) analysis for an acid-curd Spanish cheese:
872 Afuega'l Pitu atroncau blancu and roxu (PDO). *Food Hydrocolloids, 142*, 108720.
873 Reid, D. S., & Yan, H. (2004). Rheological, melting and microstructural properties of cheddar and
874 mozzarella cheeses affected by different freezing methods. *Journal of food quality, 27*(6), 436-
875 458.

Ribero, G. G., Rubiolo, A. C., & Zorrilla, S. E. (2009). Microstructure of Mozzarella cheese as affected by the immersion freezing in NaCl solutions and by the frozen storage. *Journal of food engineering, 91*(4), 516-520.

Seighalani, F. Z. B., & Joyner, H. (2019). Wear: A new dimension of food rheological behaviors as demonstrated on two cheese types. *Journal of Food Engineering, 263*, 337-340.

Shahbandeh, M. (2024). Market value of cheese worldwide from 2019 to 2032. In (Vol. 2024, pp. Cheese market value worldwide 2019-2032).

Sharma, P., Munro, P. A., Dessev, T. T., & Wiles, P. G. (2016). Shear work induced changes in the viscoelastic properties of model Mozzarella cheese. *International Dairy Journal, 56*, 108-118.

Sommer, H. (1928). The freezing point of Cheddar cheese: Injury of cheese by freezing. *Journal of Dairy Science, 11*(1), 9-17.

Timlin, M., Brodkorb, A., Harbourne, N., O'Callaghan, T. F., Drouin, G., Pacheco-Pappenheim, S., Hennessy, D., O'Donovan, M., Pierce, K. M., & Corrigan, B. M. (2024). The impact of seasonal calving systems with varying pasture allowance on Cheddar cheese composition, nutritional quality and ripening characteristics. *Journal of Dairy Science*.

To, C. M., Vermeir, L., Rebry, F., Kerkaert, B., Van der Meeren, P., & Guinee, T. P. (2020). Impact of freezing on the physicochemical and functional properties of low–moisture part–skim mozzarella. *International Dairy Journal, 106*, 104704.

Tomaszewska-Gras, J., Cais-Sokolińska, D., Bierzuńska, P., Kaczyński, Ł. K., Walkowiak, K., & Baranowska, H. M. (2019). Behaviour of water in different types of goats' cheese. *International Dairy Journal, 95*, 18-24.

Tunick, M. H. (2010). Activation energy measurements in rheological analysis of cheese. *International Dairy Journal, 20*(10), 680-685.

Tunick, M. H. (2011). Small-strain dynamic rheology of food protein networks. *Journal of agricultural and food chemistry, 59*(5), 1481-1486.

Udyarajan, C. T., Horne, D. S., & Lucey, J. A. (2007). Use of time–temperature superposition to study the rheological properties of cheese during heating and cooling. *International journal of food science & technology, 42*(6), 686-698.

Van Hekken, D., Tunick, M., & Park, Y. (2005). Effect of frozen storage on the proteolytic and rheological properties of soft caprine milk cheese. *Journal of Dairy Science, 88*(6), 1966-1972.

Verdini, R. A., Zorrilla, S., & Rubiolo, A. C. (2005). Effects of the freezing process on proteolysis during the ripening of Port Salut Argentino cheeses. *International Dairy Journal, 15*(4), 363-370.

Wang, Q., Espert, M., Hernández, M., Salvador, A., & Sanz, T. (2024). Effect of cellulose ether emulsion and oleogel as healthy fat alternatives in cream cheese. Linear and nonlinear rheology, texture and sensory properties. *Food Hydrocolloids, 150*, 109740.

Wang, X., Li, Y., & Zhao, Z. (2023). Freezing-induced changes in goat cheese: Effect of freezing rate, storage and freeze–thaw cycles. *International Journal of Dairy Technology, 76*(2), 436-441.

Wiśniewska, K., Grześkiewicz, A., Jankowska, A., & Reps, A. (2012). Feasibility of frozen storage of Gouda cheese.

Yildirim-Mavis, C., Ozmen, D., Yakisik, E., Toker, O. S., Palabiyik, I., & Kaner, O. (2022). Evaluation of kashar cheese meltability by tack and large amplitude oscillatory shear (LAOS) tests. *International Dairy Journal, 127*, 105242.

Yildirim-Mavis, C., Yilmaz, M. T., Dertli, E., Arici, M., & Ozmen, D. (2019). Non-linear rheological (LAOS) behavior of sourdough-based dough. *Food Hydrocolloids, 96*, 481-492.